energies

MDPI

Article

Integrated Vapor Compression Chiller with Bottoming Organic Rankine Cycle and Onsite Low-Grade Renewable Energy

Muhammad Tauseef Nasir [1], Michael Chukwuemeka Ekwonu [1], Javad Abolfazali Esfahani [1,2,3,*] and Kyung Chun Kim [1,*]

[1] School of Mechanical Engineering, Pusan National University, Busan 46241, Korea; tauseef@pusan.ac.kr (M.T.N.); mcekwonu@pusan.ac.kr (M.C.E.)
[2] Mechanical Engineering Department, Ferdowsi University of Mashhad, Mashhad 91775-1111, Iran
[3] Center of Excellence on Modelling and Control Systems (CEMCS), Ferdowsi University of Mashhad, Mashhad 91775-1111, Iran
* Correspondence: Abolfazl@um.ac.ir (J.A.E.); kckim@pusan.ac.kr (K.C.K.); Tel.: +82+51-510-1536 (K.C.K.)

Abstract: The present study offers a scheme to improve the performance of existing large-scale chillers. The system involves raising the temperature of the chiller's cooling water stream using renewable energy sources by incorporating an organic Rankine cycle (ORC). The thermal analysis was conducted by raising the temperature of one-third of the approximately 200 ton chiller's cooling water. The investigation was considered for ORC evaporator inlet temperature of 90~120 °C by the step of 10 °C. Various working fluids for the different ORC evaporator inlet temperatures were examined. Sensitivity analyses conducted on the degree of superheating, degree of subcooling, condenser saturation temperature, pinch point temperature differences of the ORC evaporator and condenser, and the mass flowrates of the heating and cooling streams were also reported. Genetic algorithm was employed to carry out the optimization. The best options for the ORC working fluid at the heating source ORC evaporator inlet temperatures of 90 °C was found to be DME, presenting an improvement of 48.72% in comparison with the rated coefficient of performance (COP) value of the VCC, with a renewable energy input requirement of 710 kW. At the heat source temperatures of 100 °C and 110 °C, butene, which presented an improvement in the COP equal to 48.76% and 68.85%, respectively, with the corresponding renewable energy requirements of 789.6 kW and 852 kW, was found to be the ideal candidate. Meanwhile, at the heat source inlet temperature of 120 °C, R1233zd (E), representing an improvement of 140.88% with the renewable energy input of around 1061 kW, was determined to be the most favorable ORC working fluid candidate.

Keywords: vapor compression chillers; organic Rankine cycle; heating ventilating and air conditioning; efficient energy system; renewable energy integration

check for updates

Citation: Tauseef Nasir, M.; Chukwuemeka Ekwonu, M.; Esfahani, J.A.; Kim, K.C. Integrated Vapor Compression Chiller with Bottoming Organic Rankine Cycle and Onsite Low-Grade Renewable Energy. *Energies* **2021**, *14*, 6401. https://doi.org/10.3390/en14196401

Academic Editors: José L. Bernal-Agustín and Dino Musmarra

Received: 13 August 2021
Accepted: 4 October 2021
Published: 7 October 2021

Publisher's Note: MDPI stays neutral with regard to jurisdictional claims in published maps and institutional affiliations.

Copyright: © 2021 by the authors. Licensee MDPI, Basel, Switzerland. This article is an open access article distributed under the terms and conditions of the Creative Commons Attribution (CC BY) license (https://creativecommons.org/licenses/by/4.0/).

1. Introduction

The modern-day rapid development of humanity as a whole and the burning of fossil fuels has caused an enormous strain on the environment [1,2]. Therefore, with all determination, the Paris Accord [3] was proposed and duly signed by 196 signatories at Paris, France on 12 December 2015 and came into effect on 4 November 2016. The aim at the summit was to restrain global warming to under 2 °C or, ideally, to below 1.5 °C. The agreement was signed to concert a global effort to ebb the harmful and catastrophic effects of global warming.

Under such circumstances, air conditioning, an important utility, particularly in urban areas, is estimated to consume approximately 30–40% of generated electricity [4]. Furthermore, according to [5], the United States consumes the same amount of power, for cooling alone, as the whole of continent of Africa. In China, homes with refrigerators rose from 7% in 1995 to 95% in 2007. Moreover, the growth in the cooling demands of commercial

buildings will surpass that of a residential building owing to the rapid development of humanity [6].

Therefore, the reduction in the electricity consumption of air conditioners, could aid in providing considerable relief to the grave global warming issue. Realizing the importance of this issue, several types of research were conducted. The overview of this research can be found in [7–11]. The most common technology used for cooling air conditioning and refrigeration is the vapor compression cycle technology (VCC) [12], and it is used as an integral part of HVAC [13] systems.

The heat rejected from the condenser of the VCC can be used in several ways to enhance the COP of the VCC. In this regard, Gong et al. [14] proposed a dual air and water condenser cooling technique to enable the efficient working of a VCC for cooling and heating air conditioning. The experimental investigations realized a maximum COP of 6. Furthermore, Sivaram et al. [15] performed experiments for a 1.5 ton air conditioner whose condenser heat was used to heat water. They reported that, for heating 88 liters of water up to 37 °C, the COP increased. After that, however, the COP decreased more than that of the rated COP. Apart from this, Su et al. [16] modelled the waste heat recovery of condenser heat by using an inversion method. They used temperature, the mass flow rate of cold water, hot water, and air from a retrofitted system for modelling and studying the heat transfer characteristics of heat recovery. Moreover, Jiang et al. [17] conducted a dynamic study of the heat recovery system based on an experimental setup. The performance of the electronic expansion valve and thermostatic expansion valves were also compared. They reported that the heat recovery system costs were heavy in terms of COP at the starting phase, but, on average, it improved the COP. Moreover, the electronic expansion valve was claimed to be better in terms of stability and energy performance. Other than this, Naldi and Zanchini [18] performed a theoretical dynamic analysis of a VCC whose function was to provide cooling air conditioning and domestic hot water via condenser waste heat recovery. For the weather conditions of Bologna, Italy, the seasonal saving was reported to be around 30% in comparison with the traditional cooling air conditioning and boiler for heating water.

With regards to using the absorption refrigeration cycle, to harness this waste heat, Kairouani and Nehdi et al. [19] conducted a thermal investigation of a system that used the waste heat from the VCC to vaporize the refrigerant in the evaporator section of the absorption refrigeration cycle. From their evaluations, the increase in the COP for the system was around 37–54% in comparison with the VCC. Similarly, Cimsit and Ozturk et al. [20] performed the thermal evaluation using the NH_3-water and H_2O-water absorption refrigeration cycles to utilize the waste heat from the VCC. The working fluids, R134a, R410a, and NH_3, were used in the VCC. The reduction in the energy consumption for the presented system was found to be 48–51%. A thermal evaluation of a similar system was performed by Garimela et al. [21], wherein they considered the use of CO_2 as the working fluid of the VCC and H_2O-LiBr absorption chiller. They reported a reduction in electricity consumption by 31%.

Another technology that can be used to harness the waste heat from the condenser of the VCC is the organic Rankine cycle (ORC). It is a technology that is based on the conventional Rankine cycle, except that its working fluids are mostly organic compounds whose typical boiling points are less than that of water. That is, the normal boiling point of water at atmospheric pressure is 99.974 °C, whereas, for example, the boiling point of one of the popular working fluids, R245fa, at atmospheric pressure is 15.139 °C [22]. Owing to this characteristic of having a lower boiling point, ORC can utilize low grade heat energy for electricity production. The general information regarding ORC applications can be found in [23–26]. Similarly, the research regarding working fluids can be sought from [27–29] and, regarding components, from [30–33].

To recover the VCC condenser heat, Asim et al. [34] proposed a system that used an ORC to recuperate the condenser heat rejected by the VCC. They reported isobutane-R123 as the most viable VCC-ORC combination, with the COP recorded as enhancing from the

rated value of 3.10 to 3.54. Khalilzadeh et al. [35] proposed and analyzed a system to reduce the power consumption of a cascade refrigeration cycle using solar energy input and an ORC. The evaporator temperature of the lowest most VCC was recorded as −55 °C. In their research, the temperature of the condenser cooling stream was enhanced using solar energy to power a high-temperature ORC. The ORC power generated was used to reduce the power consumption of the VCC and provide heat. The exergetic efficiency and increase in total investment cost of the system were found to be 84.53% and 20%, respectively.

The utilization of the ORC as the prime mover to convert the heat energy available from any source, such as solar, geothermal, biomass, waste heat, etc., into mechanical power, which can be used to run the compressor of the VCC, was also explored. Considering this perspective, Nasir and Kim [36] evaluated the thermal performance of such a system considering different working fluids. For a hot water source of 100 °C and 1.5 atm, the R134a ORC-isobutane VCC was reported to be the ideal working fluid candidate with an optimized COP of 0.281. In another study by Nasir et al. [37], considering the UA values of the heat exchanger as well, R245fa ORC-R600a VCC was found to be the best working fluid candidate at the ambient temperature of 30 °C and 35 °C. For the ambient temperature of 40 °C, on the other hand, the ideal combination was reported to be R600a ORC-R245fa VCC. Apart from this, Molés et al. [38] also performed a thermal evaluation of several environment-friendly working fluids. They reported COP variation in the range from 0.3 to 1.10. The overview of these studies is presented in Table 1.

Table 1. Summary of studies performed on enhancing the efficiency of vapor compression chillers.

Ref.	Suggested Improvement	Results/Remarks
[14]	Dual air and water condenser cooling technique	Max. COP of 6
[15]	Condenser heat to heat water	Initially the COP increased, but afterwards it decreased
[16]	Modelled the waste heat recovery of condenser heat by using an inversion method. Analyzed on a retrofitting case	There was 50% less heat exchange with 80% pressure loss
[17]	Dynamic electronic expansion valve and thermostatic valve expansion valves compared	Overall, the COP improved. Electronic expansion valve better than thermostatic expansion valve
[18]	Waste heat used for heating water	Seasonal savings of approximately 30%
[19]	Utilization of the VCC waste heat to vaporize the refrigerant of the absorption chiller	37 to 54% improvement in COP
[20]	VCC waste heat utilization for vaporizing the refrigerant in the absorption chiller. LiBr-water and NH_3-water absorption chillers compared	Electrical energy consumption was 48–51%. LiBr-water absorption chiller slightly better than NH_3-waster absorption chiller
[21]	VCC waste heat from CO_2 VCC used to vaporize the refrigerant in the evaporator of LiBr-water absorption chiller	Reduction of electricity consumption by 31%.
[30]	VCC waste heat utilization to power an ORC	Isobutane VCC-R123 ORC was the best combination. COP enhanced from 3.10 to 3.54
[31]	Improvement in the cascade refrigeration system using solar energy and ORC	Exergetic efficiency was 84.53%. Increase in total investment cost by 20%
[32]	ORC expander coupled with compressor of VCC	R134a ORC-R600a VCC best combination. Optimized COP of 0.281
[33]	ORC expander coupled with compressor of VCC	R245fa ORC-R600a VCC best combination in case when ambient temperature was 30 and 35 °C. R600a ORC-R245fa VCC for ambient temperature of 40 °C
[34]	ORC expander coupled with compressor of VCC	Max. COP of 1.10

Keeping in mind the previous research conducted to improve the performance of the VCC, advancement was proposed in this paper with an aim towards the partial reduction of VCC power consumption. In particular, through consideration of retrofitting the case, that is, the VCC, as well as the cooling tower, to be not changed at all. The proposed system was based on increasing the temperature of some parts of the VCC condenser cooling stream by using onsite renewable energy sources. By using this part of the stream, the ORC runs and generates electricity for the partial reduction of VCC power consumption, which is the main difference from our previous work [36,37] in which the VCC compressor was directly linked with the ORC expander. The rest of the VCC condenser stream is used for cooling the ORC condenser to lower the temperatures of its heated streams. The proposed scheme can be adopted by modifying the cooling circuit of the existing VCC, without altering the VCC system or the cooling tower itself. Therefore, by utilizing such a system, a more economically viable system could be attained. To the best of our knowledge, the research regarding the improvement of existing industrial chillers using the VCC condenser heat and renewable energy sources at low-grade heat sources was not previously conducted. The low-grade heat is categorized as the heat with a temperature in the range of 95–120 °C [39]. Such temperatures can be achieved by using solar collectors, such as flat plate collectors, evacuated tube collectors, and hydrothermal reservoirs [39]. Other than this, onsite biomass sources, such as the human or animal waste, or discarded papers etc., can be used for providing the heat to the ORC for operation to enhance sustainability. The energetic analysis of the proposed novel scheme was conducted, and the effect of the design parameters of the ORC were investigated. The performance of several potential working fluids was evaluated, and the best candidate was sought out.

2. Proposed System

The conventional scheme in which the water-cooled chillers are generally installed is shown in Figure 1. The chiller cooling water enters the condenser of the VCC at state J, for extracting the heat. After extracting heat, this water stream exits the condenser at state A. In a cooling tower, the cooling stream loses heat to the ambient temperature. Then, the cooling water is sent again to the condenser of the VCC at state J. An attached pump is an integral part of the cooling circuit for maintaining the flowrate.

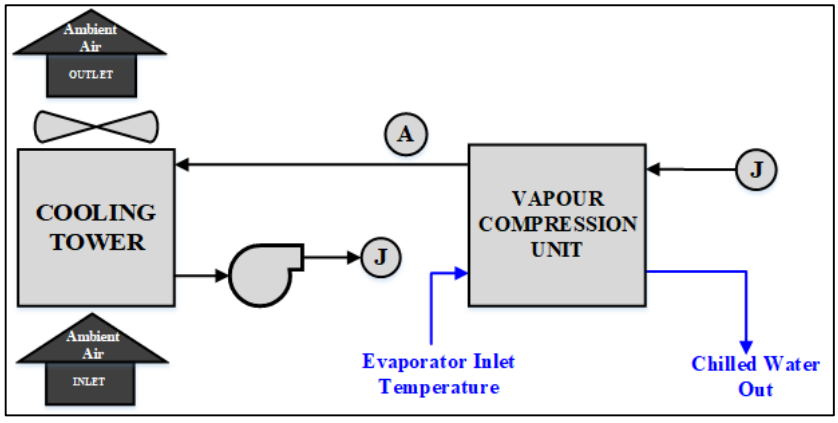


Figure 1. Conventional configuration of an air conditioning chiller.

The schematic of the proposed scheme is portrayed in Figure 2.

The VCC condenser cooling water is divided into three streams. One of the streams, denoted by X (colored red in the schematic), is sent to gain heat from renewable energy sources, such as solar, biomass, geothermal, or combinations of therein, subject to availability. The pressure of this stream is raised using pump 2 accordingly to prevent the formation of steam, as depicted by state X1, illustrated in Figure 2. The stream termed B (blue colored in the schematic) is used for cooling the ORC condenser. At the same time, the third one

is kept as it is. The stream X1, recuperates the heat rejected by the ORC condenser to reach state X1′. Then it recovers the available heat in the ORC evaporator to achieve state X1″. Renewable energy is then used to raise the temperature of the stream to the required temperature, which then enters the ORC evaporator to enable it to produce power. The three streams C, H, and I are then mixed in a heat exchanger to achieve a temperature intermediate to the temperature of the three streams at state J. The pressure of J is lowered using a throttling valve to the pre-pump 1 pressure. Afterward, supply water at state Y (yellow colored in the schematic) enters mixing heat exchanger-II and cools the temperature of this stream to the temperature at state A (Figures 1 and 2). Following this, the amount of supply water is drained using a divider and sent back to the supply. This supply water stream can be obtained from the building water supply or by any other source, such as wells or rivers. In the case of domestic hot water applications, the raised temperature of this stream could help in mitigating energy requirements even further. Finally, the stream then enters the cooling tower and goes to the VCC condenser, thereby completing the loop. The VCC, which usually gets the electric power input from the grid, now receives lower electrical power input as the ORC will share some of the burden.

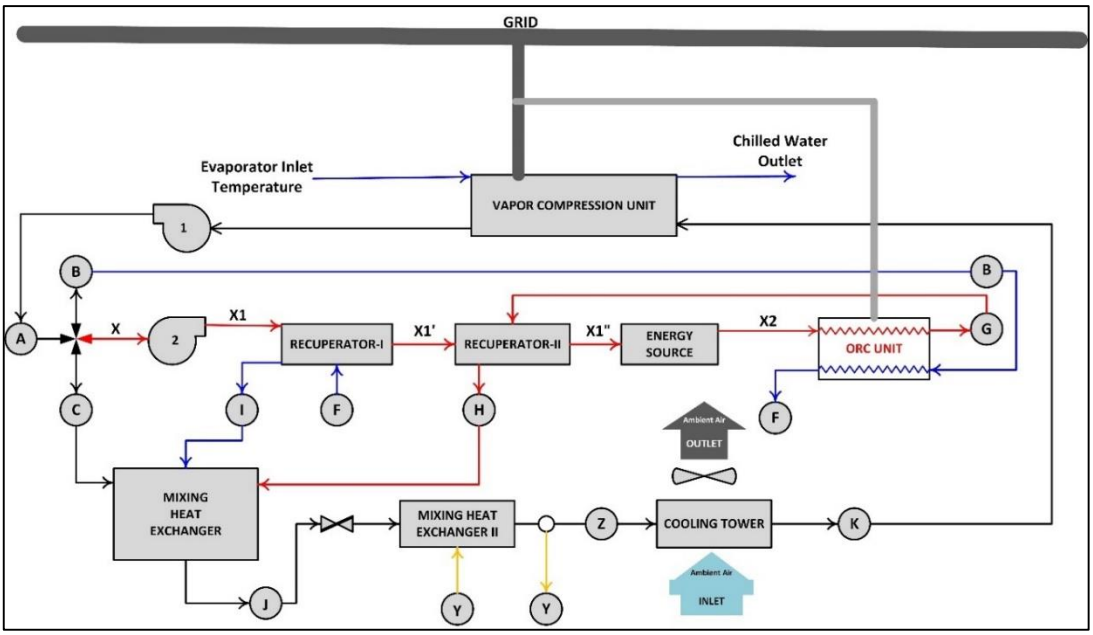


Figure 2. Schematic of the proposed scheme.

3. Thermal Analysis

In this section, the assumptions, the considered working fluids, mathematical modelling, and the solution methodology is presented.

The schematic and the T-S diagram of a simple ORC used to conduct the analysis is delineated in Figure 3. In an ORC, the working fluid boils in the evaporator from state 1 to state 2. The working fluid then expands in the expander from a higher pressure to lower pressure from state 2 to state 3. Following this, the vapor condenses from state 3 to state 4 in the condenser of the ORC. Afterward, the pump is used to raise the pressure of the working liquid from state 4 to state 1.

As a reference case to conduct the thermal analysis, operational parameters of a centrifugal chiller RCWFHA0, manufactured by LG Electronics [40], was adopted. The general parameters of this chiller are presented in Table 2.

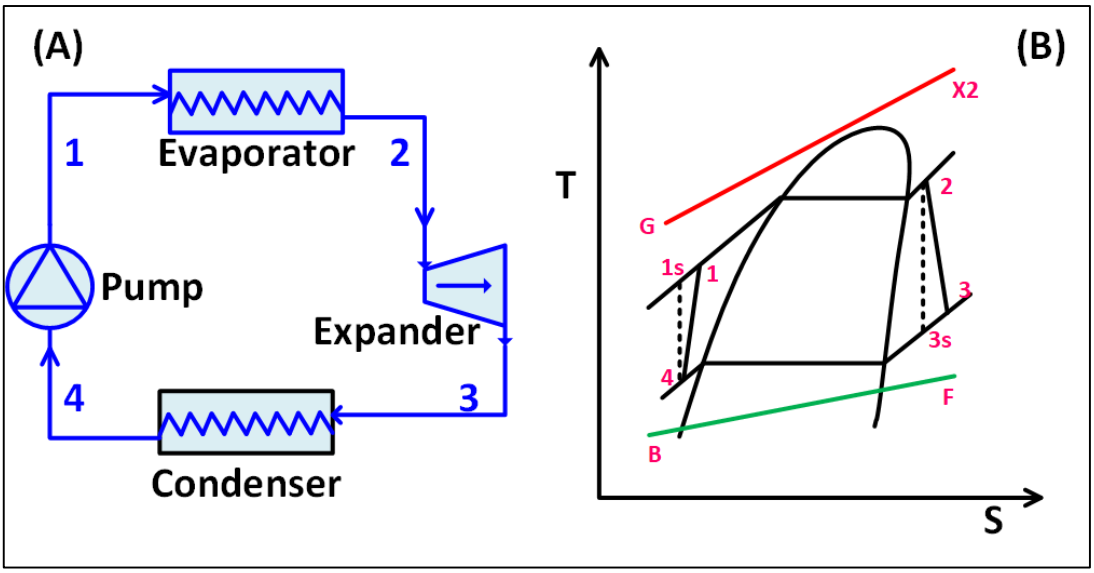


Figure 3. (**A**) schematic and (**B**) T-S diagram of the ORC.

Table 2. Specifications of the VCC adopted for this study [40].

Parameter	Value
Cooling Capacity (US-RT/kW)	200/703
Rated COP	6.7
Condenser Flow Rate (m^3/s)	35
Power Consumption at Rated Capacity and COP (kW)	(703/6.7)~105
Condenser Inlet Temperature (°C)	29.4
Condenser Outlet Temperature (°C)	35
Evaporator Inlet Temperature (°C)	12.2
Evaporator Outlet Temperature (°C)	6.7

3.1. Assumptions

The following assumptions were made to perform the analysis:

1. Steady state conditions were considered [41];
2. The frictional and pressure losses were assumed to be insignificant [42];
3. The heat losses in the system were ignored [36];
4. The isentropic efficiencies of the pump and the expander of the ORC were assumed to be 0.7 each [43];
5. The maximum boiler pressure was set to 0.85 times the critical pressure, from inferences taken from [44];
6. The recuperator efficiency was considered to be 0.9 [45];
7. The electromechanical efficiency of the electrical generator was considered to be 0.95 [46];
8. The electromechanical efficiency of the electrical motor was considered to be 0.97 [47];
9. The inlet temperature of the supply water stream (stream Y) was considered to be 15 °C.

3.2. Working Fluid Candidates

The selection of an appropriate working fluid is pivotal for the thermal performance and cost of the overall ORC system [48]. The proper selection of working fluid involves several points, including physical, chemical, safety, and health considerations [49]. There are several essential thermal properties that should be fulfilled to achieve the maximum

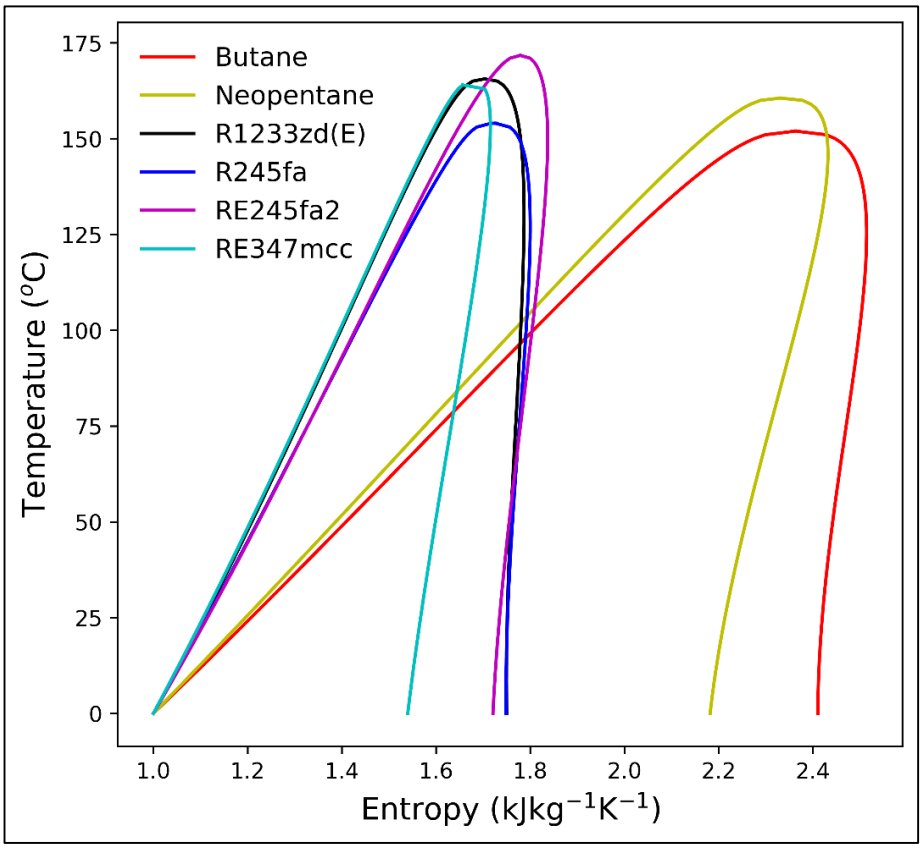
benefit, and the recommendations could be sought from the works of Bao et al. [27] and Aboelwafa et al. [48].

It was shown that thermal efficiency increases with an increase in the critical temperature [49]. Brown et al. [50] conducted a parametric study that revealed the critical temperature to be approximately 100 to 150% of the heat source to yield maximum efficiency. Chen et al. [51] claimed the maximum exergetic efficiency is reached when the critical temperature reached the heat source temperature, in the case when the condensing temperature and the reduced evaporating temperature were 40 °C and 0.85, respectively. Yang et al. [52] recommended that critical temperature can be used for screening of the working fluids for low temperature heat sources. Hærvig et al. [53] suggested the critical temperature to be 30–50 K above the heat source temperature. Similarly, Zhai et al. [54] presented a mathematical expression relating the critical temperature to heat source temperature and the pinch point temperature difference (PPTD) in the evaporator.

Keeping in view the crux of previous studies, and considering the environmental concerns, the working fluids selected for the analysis are presented in Table 3, along with their general thermal and environmental properties. Their associated TS diagrams are shown in Figure 4, which represents the slope of the temperature and saturated vapor lines. The fluids can be labeled as either wet (negative slope, for example cyclopropane), isentropic (infinite slope, for example isobutane), or dry (positive slope, for example butane) [55]. Furthermore, the critical temperatures, as well as the latent heats of vaporization/condensation, can be deduced from Figure 4.

Table 3. Thermal and environmental properties of the selected working fluids.

Working Fluid	Ref.	Critical Temperature (°C)	Critical Pressure (MPa)	Saturated Vapor Entropy Curve	ODP	GWP
Cyclopropane	[46,56]	125	5.6	Wet	0	0
DME	[47,53,56]	127	5.3	Wet	0	4
Isobutane	[51,56]	135	3.6	Isentropic	0	20
Isobutene	[51,56]	145	4	Isentropic	NA	3
Propyne	[54,56]	129	5.62	Wet	0	25
RE245cb2	[52,53,56]	134	2.89	Isentropic	0	654
Butane	[54,56]	152	3.8	Dry	0	20
Butene	[55,56]	146	4	Isentropic	NA	NA
Neopentane	[54,57]	161	3.2	Dry	0	20
Cis-butene	[54,54,56]	163	4.23	Isentropic	NA	NA
R1233zd (E)	[49,58]	166	3.6	Dry	0.0003	1
R245fa	[50,58]	154	3.65	Dry	0	820
RE245fa2	[51,54,58]	172	3.63	Dry	0	812
RE347mcc	[49,54,58]	165	2.5	Dry	0	530



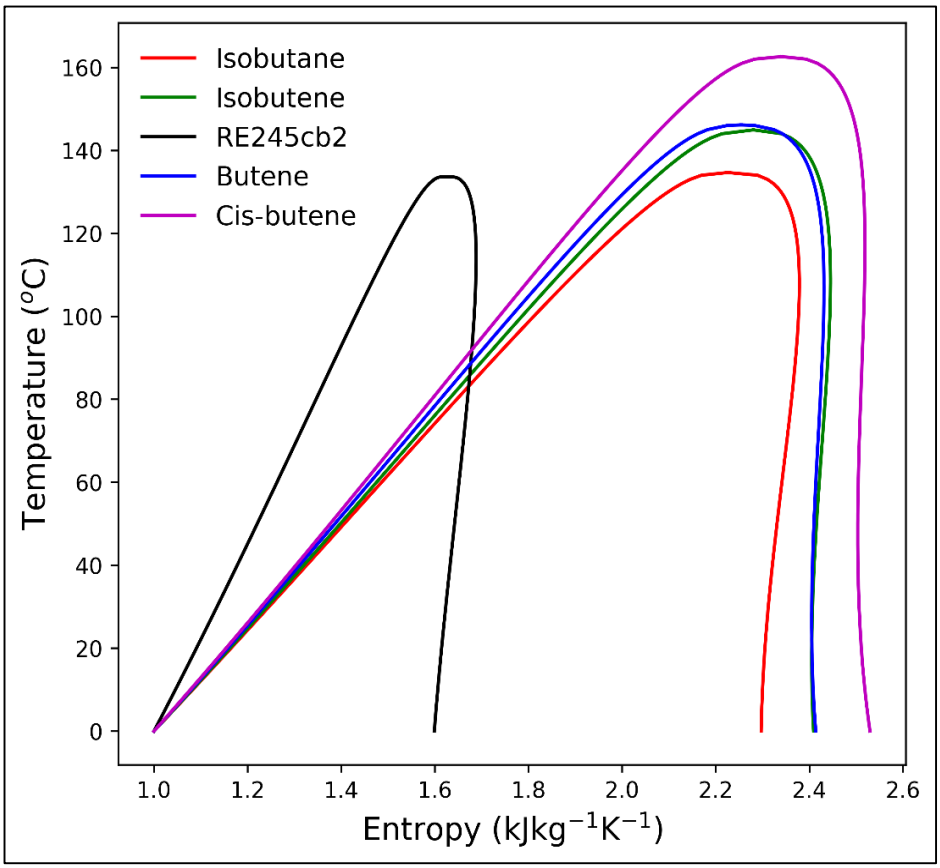


Figure 4. *Cont*.

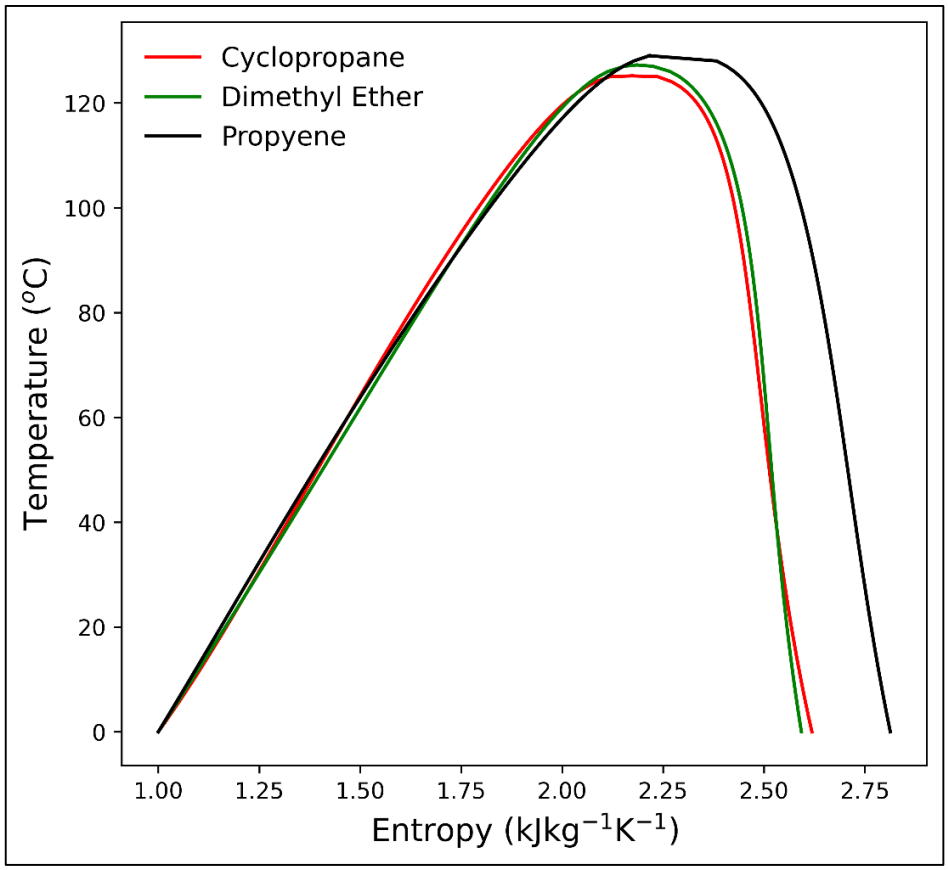


Figure 4. TS diagram of the selected working fluids (topmost: dry working fluids; middle: isentropic working fluids; and bottom: wet working fluids).

Furthermore, from the guidelines on working fluid selection provided in the discussion mentioned above, the selected working fluid are categorized in Table 4 on the basis of the heat source inlet temperature. It should be noted that several shortlisted working fluids overlap for different heat temperatures. For example, based on the recommendations from the literature, considering the critical temperature of isobutane, it can be considered a viable working fluid candidate when the heat source temperature is around 90 °C and 100 °C.

Table 4. Selection of working fluids based on heat source temperature.

ORC Evaporator Inlet Temperature (°C)	90	100	110	120
Critical Temperature Range (°C)	120–140	130–150	140–160	150–170
Working Fluids	Cyclopropane (RC 270)	Isobutene		R1233zd (E)
	Dimethyl Ether (DME)	Butene		Cis-butene
	Isobutane		Neopentane	
	Propyne		Butane	
	RE245cb2			R245fa
				RE245fa2
				RE347mcc

3.3. Mathematical Modelling

The heat transfer to the evaporator of the ORC, which enables evaporation and superheating of the working fluid, is given as:

$$\dot{Q}_{BOIL} = \dot{m}_{ORC} \times (H_2 - H_1) \tag{1}$$

The expansion across the expander, which produces work, is mathematically represented as:

$$\dot{W}_{EXP} = \dot{m}_{ORC} \times (H_2 - H_{3s}) \times 0.7 \tag{2}$$

where 0.7 is the isentropic efficiency of the expander [43].

The heat released by the ORC condenser, as the working fluid condenses, is given as:

$$\dot{Q}_{COND} = \dot{m}_{ORC} \times (H_3 - H_4) \tag{3}$$

The pump work is given as:

$$\dot{W}_{PUMP} = \left(\dot{m}_{ORC} \times (H_1 - H_{4s})\right)/0.7 \tag{4}$$

where 0.7 is the isentropic efficiency of the expander [43].

The volumetric expansion at the expander outlet is given as:

$$\dot{\forall}_3 = \frac{\dot{m}_{ORC}}{\rho_3} \tag{5}$$

Meanwhile, the heat gained by the ORC condenser cooling water is mathematically written as:

$$\dot{Q}_{F-B} = \dot{Q}_{COND} = \dot{m}_B \times c_p \times (T_F - T_B) \tag{6}$$

The temperature at point X1′ is determined as:

$$\eta_{HX} = \frac{\dot{m}_X \times c_p \times (T_{X1'} - T_{X1})}{\dot{m}_{min} \times c_p \times (T_F - T_{X1})} \tag{7}$$

where $\dot{m}_{min} = \dot{m}_B$ or $\dot{m}_X$, the minimum from either of them.

The temperature at the point I is calculated as:

$$T_I = T_F - \frac{\dot{m}_X \times c_p \times (T_{X1'} - T_{X1})}{\left(\dot{m}_B \times c_p\right)} \tag{8}$$

From the mass conservation,

$$\begin{gathered} \dot{m}_B = \dot{m}_F = \dot{m}_I; \\ \dot{m}_X = \dot{m}_{X1} = \dot{m}_{X1'} = \dot{m}_{X1''} = \dot{m}_{X2} = \dot{m}_G = \dot{m}_H \end{gathered} \tag{9}$$

The temperature at point X1″ is determined as:

$$\eta_{HX} = \frac{\dot{m}_X \times c_p \times (T_{X1''} - T_{X1'})}{\dot{m}_X \times c_p \times (T_G - T_{X1'})} \tag{10}$$

The temperature at point H is given as:

$$T_H = T_G - \frac{\dot{m}_X \times c_p \times (T_{X1''} - T_{X1'})}{\left(\dot{m}_X \times c_p\right)} = T_G - T_{X1''} + T_{X1'} \tag{11}$$

The temperature at point G is calculated from the following Equation:

$$T_G = T_{X1''} - \frac{\dot{Q}_{BOIL}}{\left(\dot{m}_X \times c_p\right)} \tag{12}$$

The temperature at point J is determined as:

$$T_J = \frac{\left[\left(\dot{m}_C \times T_C\right) + \left(\dot{m}_I \times T_I\right) + \left(\dot{m}_H \times T_H\right)\right]}{\left(\dot{m}_J\right)} \tag{13}$$

The additional supply water mass flow required to lower the temperature to avoid extra load at the cooling tower is mathematically given as:

$$M_Y = \frac{\left(T_j \times \dot{m}_J\right) - \left(T_Z \times \dot{m}_J\right)}{\left(T_Z - T_Y\right)} \tag{14}$$

The percentage of reduction for compressor work for the VCC is given as follows:

$$\%\ RCP = 100 - \left(\frac{\dot{W}_{COMP} - \left(\left(0.95 \times \dot{W}_{EXP}\right) - \left(\frac{\dot{W}_{PUMP}}{0.97}\right) \right)}{\dot{W}_{COMP}} \right) \times 100 \tag{15}$$

where 0.95 and 0.97 are the generators' electromechanical efficiency [38] and motor's electromechanical efficiency, respectively [43]. For the design analysis, in Equation (15), $\dot{W}_{COMP}$, the VCC compressor work requirement is treated as constant, having the values of 105 kW [40].

The rate of heat gained by the renewable energy sources is mathematically described as:

$$\dot{Q}_{ren} = \dot{m}_X \times c_p \times \left(-T_{X2} - T_{X1''}\right) \tag{16}$$

3.4. Methodology

The analysis was conducted using the MATLAB programming environment, and the values of the working fluid properties were evaluated via Refprop version 9.1 [22]. Thermal equations are non-linear in nature because of the working fluid properties. Furthermore, these equations are also linked and have interdependent behavior. Therefore, the algorithm for assessing the state points of the ORC was adopted and modified accordingly from previous work [36]. The flow chart of the algorithm to estimate the state properties and ORC mass flow rate for baseline conditions in Figure 3, and the equations mentioned in Section 3.3, is presented in Figure 5.

After determining the ORC properties and flow rate, the other necessary calculations are conducted to determine the T_F, T_G, $T_{X1'}$, $T_{X1''}$, T_I, T_H, T_J, and the performance indices RPC, $\dot{Q}_{ren}$, and M_Y from Equations mentioned in Section 3.3.

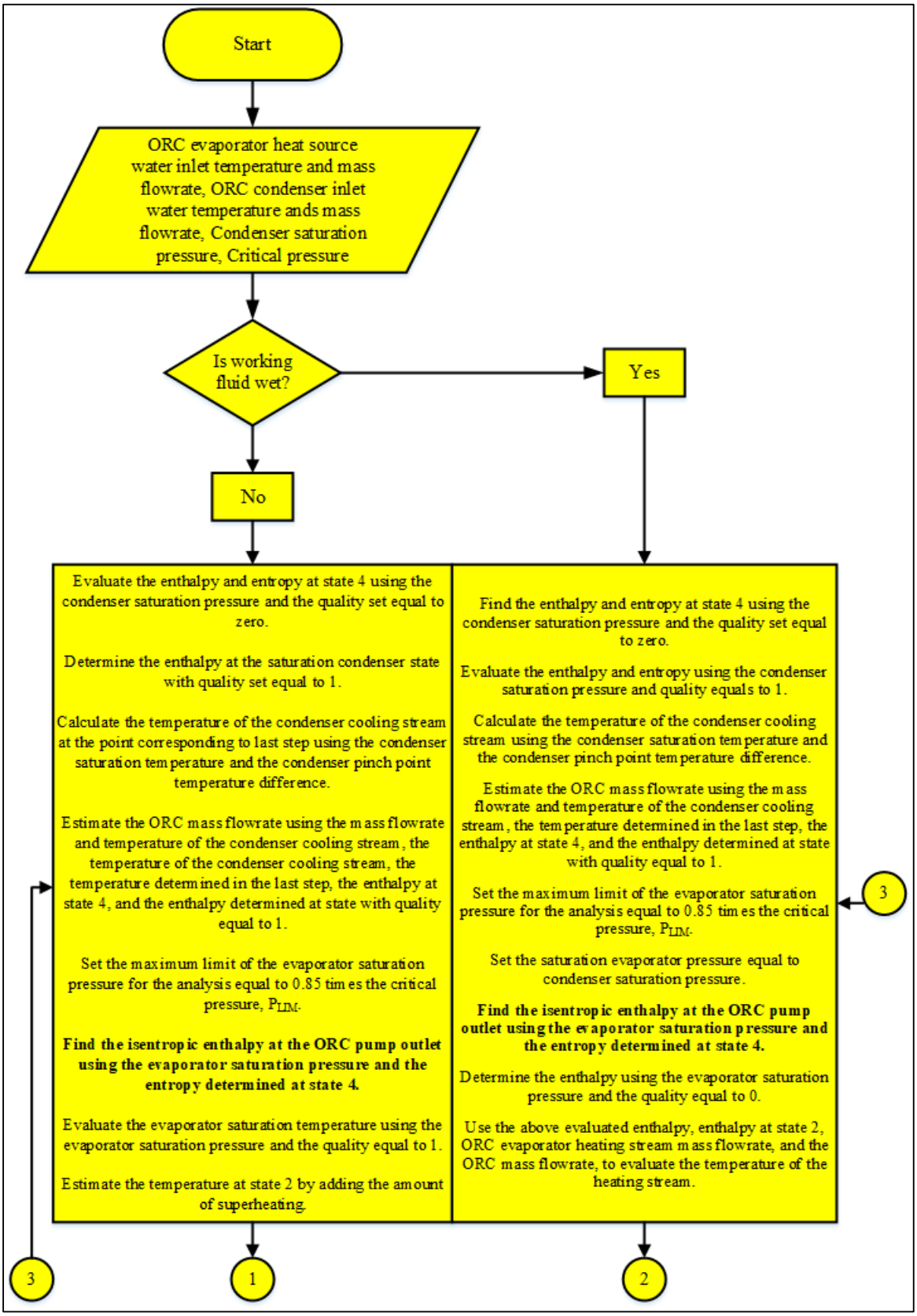


Figure 5. *Cont.*

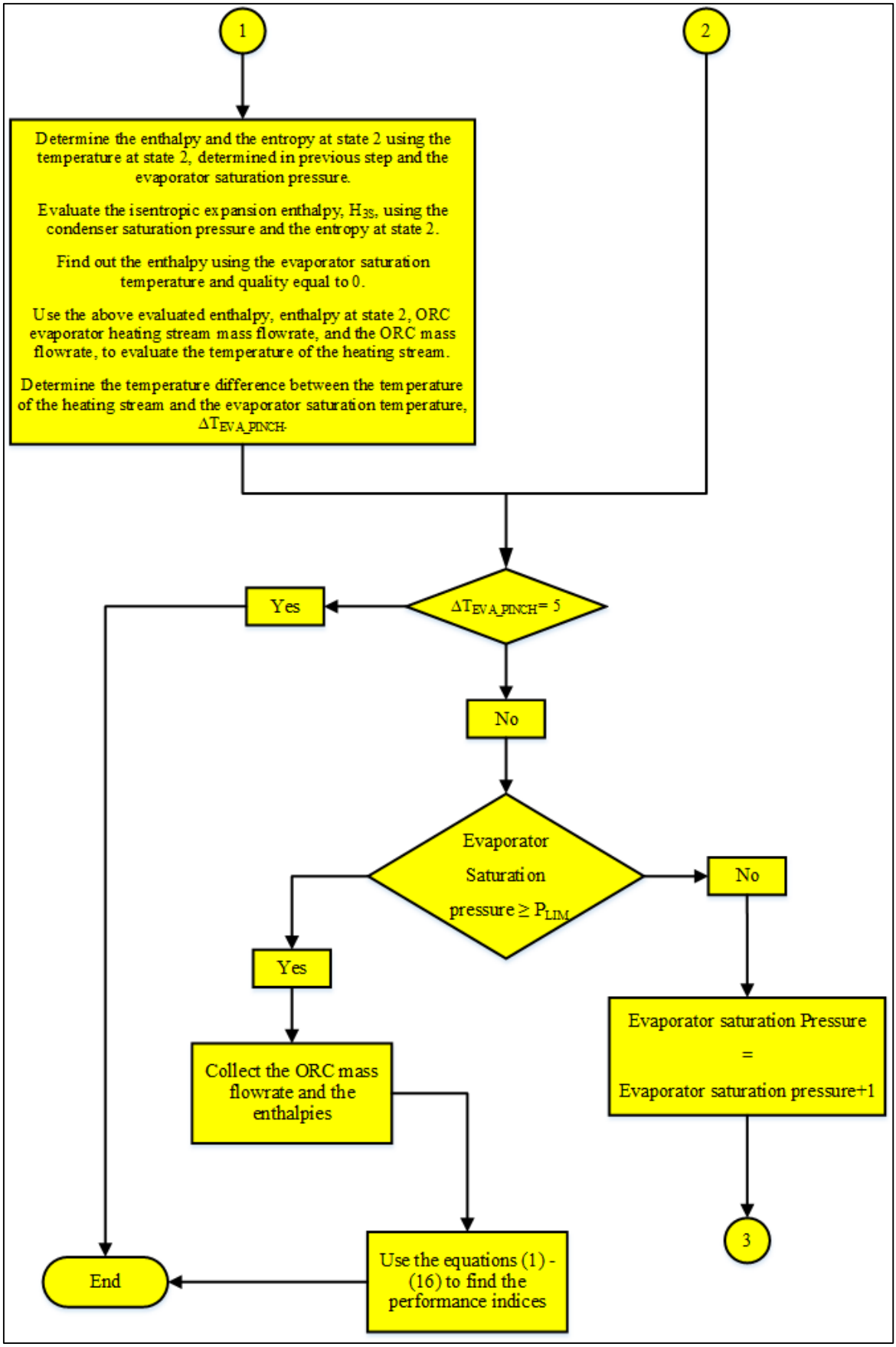


Figure 5. Flowchart for acquiring the ORC state properties and mass flow rate.

3.5. Validation

The codes developed in this case were validated with the work of Tchanche et al. [47]. In [47], the software used was Engineering Equation Solver, while in the present case, MATLAB, in parallel with the Refprop, was used. The validation results are shown in Table 5. The maximum difference was 2.15%, while the ammonia had a 0.55% difference. This confirmed the accuracy of the present work. Furthermore, the errors can be attributed to the change of simulation software; that is, presently, MATLAB with REFPROP was used, whereas in [47], the software Engineering Equation Solver was used.

Table 5. Validation of the present simulation with Ref. [47], considering the conditions of Ref. [47].

Working Fluid	Parameters [38]								$\dot{W}_{EXP}$	$\dot{W}_{EXP}$	%Diff
	Exp. Isentropic Efficiency	Pump Isentropic Efficiency	Electrotechnical Efficiency of Generator	T_{X2}	$\dot{m}_{X2}$	$\dot{m}_{ORC}$	T_{COND}	ΔT_{PINCH}			
	(%)	(%)	(%)	(°C)	(kg/s)	(kg/s)	(°C)	(°C)	(kW) [47]	(kW) (Present Study)	
R134a	0.7	0.8	0.63	90	0.75	0.244	35	6	2	2.036	1.8%
R152a	0.7	0.8	0.63	90	0.82	0.154	35	6	2	2.043	2.15%
Methanol	0.7	0.8	0.63	90	0.99	0.034	35	6	2	2.007	0.35%
Ammonia	0.7	0.8	0.63	90	0.90	0.037	35	6	2	2.011	0.55%

4. Results and Discussion

In this section, firstly, the analysis at the baseline operating parameters is presented, then a sensitivity analysis is performed. The sensitivity analysis was performed to assess the effects of varying the design parameters, ORC boiler superheat, ORC condenser saturation temperature, ORC condenser degree of subcool, ORC evaporator PPTD, the ORC condenser PPTD, the heating source mass flowrate variation, and the cooling source mass flowrate on the reduction in electrical power consumption of the VCC, the renewable energy input, and the required supply water mass flow rate to lower the temperature to the specified cooling tower inlet temperature. The values of the baseline conditions, and the range of the operational parameters for the sensitivity analysis, which were partially adapted from the authors' previous work [29], are presented in Table 6.

Table 6. Baseline operating conditions and the range of parameters.

Parameter	Baseline Value	Range
ORC boiler superheat (°C)	1 (or adjusted accordingly for the wet working fluids to ensure the prevention of isentropic expansion outlet occurring in the wet region)	1–10
ORC condenser saturation temperature (°C)	50	50–60
ORC condenser degree of subcool (°C)	0	0–5
ORC evaporator PPTD (°C)	5	5–10
ORC condenser PPTD (°C)	5	5–10
Heat source mass flowrate (kg/s)	11.67	0.1–1 (×11.67)
Cooling mass flowrate (kg/s)	11.67	0.1–1 (×11.67)

4.1. Baseline Results

The baseline results of the current study for all the working fluid candidates are shown in Table 7. From the perspective of having the maximum reduction in the work input (*RCP*), RE245cb2 was found to be the best working fluid at the ORC heat source inlet temperatures of 90 °C and 100 °C. Neopentane and RE347mcc, on the other hand, were found to present the best results at the heat source temperatures of 110 °C and 120 °C,

respectively. Their corresponding values of the *RCP* were determined to be 21.74%, 29.94%, 38.32%, and 46.74%. Considering the minimum renewable energy input, DME, propyne, butene, and cis-butene were the ideal candidates. These working fluids displayed the values of 694.82 kW, 755.10 kW, 824.66 kW, and 880.55 kW, respectively, at the respective heat source inlet temperatures of 90 °C, 100 °C, 110 °C, and 120 °C. The water supply temperatures were found to be approximately in between 8–8.3 kg/s, 8.7–9 kg/s, 9.4–9.8 kg/s, and 10–10.8 kg/s at the ORC heat source inlet temperatures of 90 °C, 100 °C, 110 °C, and 120 °C, respectively.

Table 7. Baseline results at various heat source temperatures.

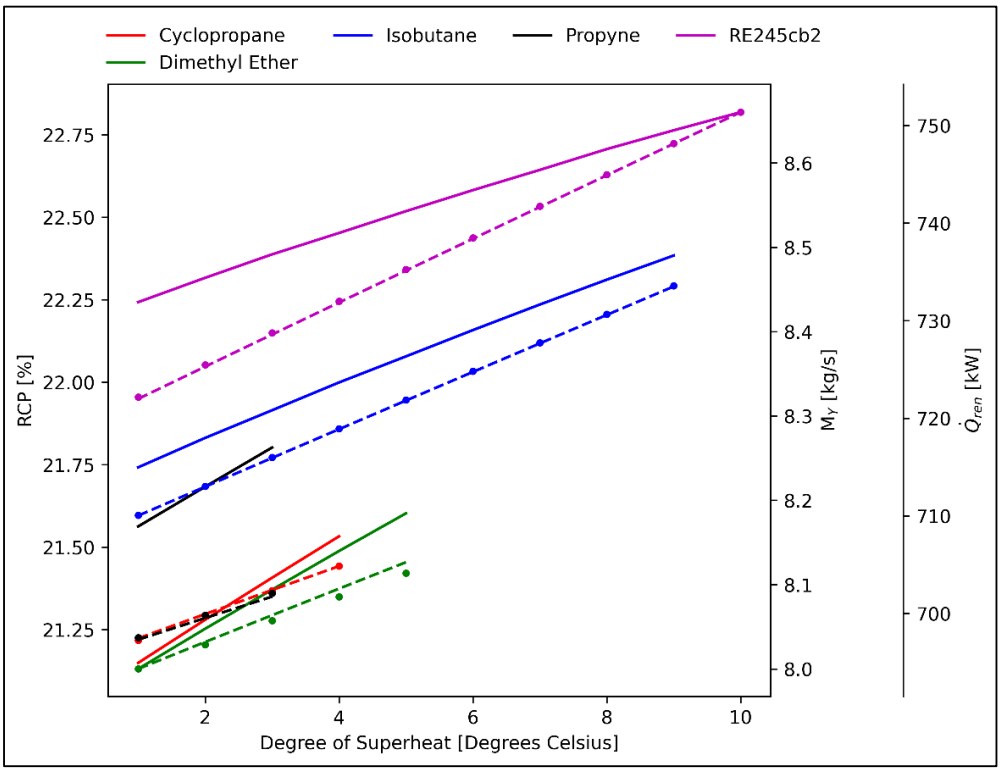
Working Fluid	Wexp (kWe)	Wpump (kWe)	ORC Mass Flowrate (kg/s)	Volumetric Expansion at the Expander Outlet (m^3/s)	RCP (%)	$\dot{Q}_{ren}$ (kW)	M_Y (kg/s)
Heat Source Temperature = 90 °C							
Cyclopropane	25.74	3.39	1.35	0.0528	21.15	697.24	8
DME	25.44	2.97	1.36	0.0580	21.13	694.82	8
Isobutane	25.57	2.62	1.63	0.0971	21.74	710.05	8.2
Propyne	25.50	2.72	1.14	0.0572	21.56	710.05	8
RE245cb2	25.43	1.95	3.58	0.1310	22.24	722.13	8.3
Heat Source Temperature = 100 °C							
Butene	34.02	3.02	1.47	0.1068	29.52	764.12	8.7
Isobutane	34.60	3.98	1.63	0.0985	29.16	774.35	8.8
Isobutene	34.13	3.12	1.48	0.1049	29.53	766.71	8.8
Propyne	35.10	4.26	1.14	0.0578	29.05	755.10	8.6
RE245cb2	34.45	3.01	3.58	0.1334	29.94	790.90	9
Heat Source Temperature = 110 °C							
Isobutene	42.58	4.42	1.48	0.1059	36.44	827.81	9.4
Butene	42.44	4.29	1.47	0.1078	36.40	824.66	9.4
Neopentane	43.51	3.18	1.73	0.1782	38.32	865.53	9.8
Butane	42.89	3.73	1.46	0.1285	37.22	838.80	9.5
Heat Source Temperature = 120 °C							
R1233zd (E)	50.12	3.11	2.74	0.1888	44.92	893.75	10
Cis-butene	45.58	4.01	1.34	0.1358	43.79	880.55	10
Neopentane	52.12	4.29	1.73	0.1814	45.47	935.53	10.5
Butane	51.04	5.03	1.46	0.1300	43.74	901.47	10.2
R245fa	50.27	3.72	2.79	0.1585	44.40	901.00	10.2
RE245fa2	50.99	2.41	2.83	0.2494	46.38	920.71	10.4
RE347mcc	51.72	2.68	3.84	0.3084	46.74	959.61	10.8

4.2. Sensitivity Analysis

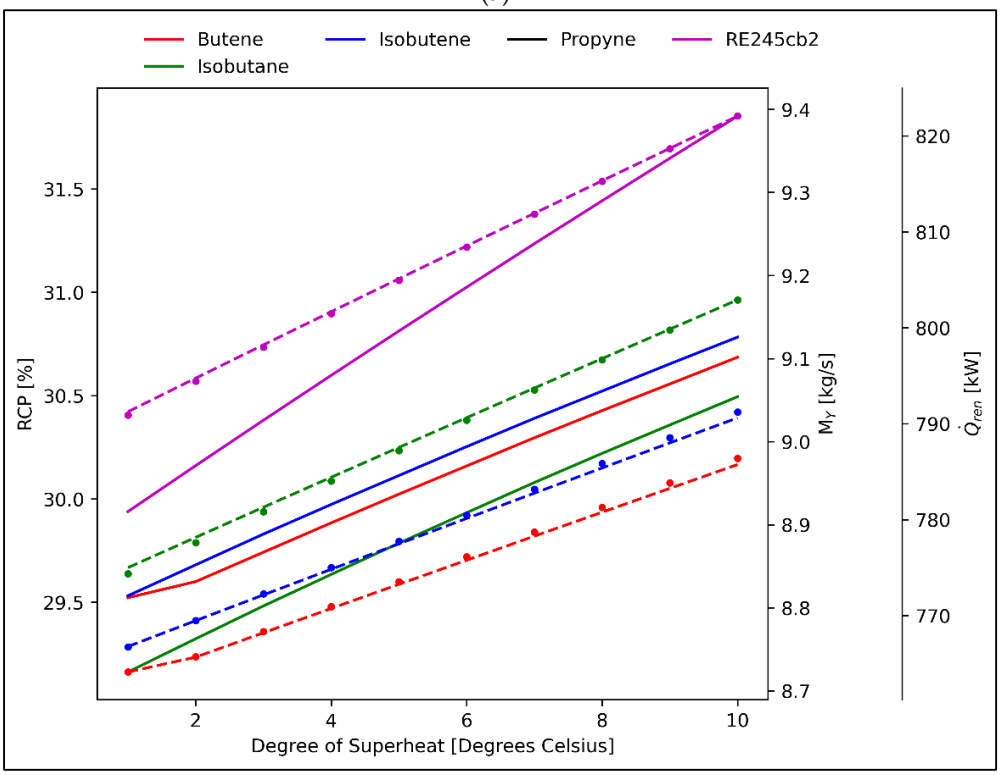
For the sensitivity analysis, the selected design parameters were the degree of evaporator superheating, the condenser degree of subcooling, the condenser saturation temperature, the PPTDs of the ORC evaporator and the condenser, and the heat and cold sources fluid mass flowrates. It should be noted that having higher values of the reduction of the VCC compressor power work input, termed as *RCP*, is beneficial. Meanwhile, it is more fruitful to have smaller values of renewable energy requirements. A lesser amount of renewable energy input points towards a smaller solar collector area, a smaller capacity biomass boiler, or, in general, smaller renewable energy harnessing equipment. Similarly, having lower values of the mass flowrate of the stream Y, which is representative of the system's cooling arrangement, is also beneficial from an economic point of view. It should be noted that, when a particular design parameter is analyzed, the rest of the design parameters are kept constant.

4.2.1. Effect of ORC Evaporator Superheat

The impacts of the ORC evaporator superheat on the reduction in power consumption, the renewable energy input, and the supply water mass flowrate at the stream Y are presented in this section. The trends for these performance indices are shown in Figure 6.

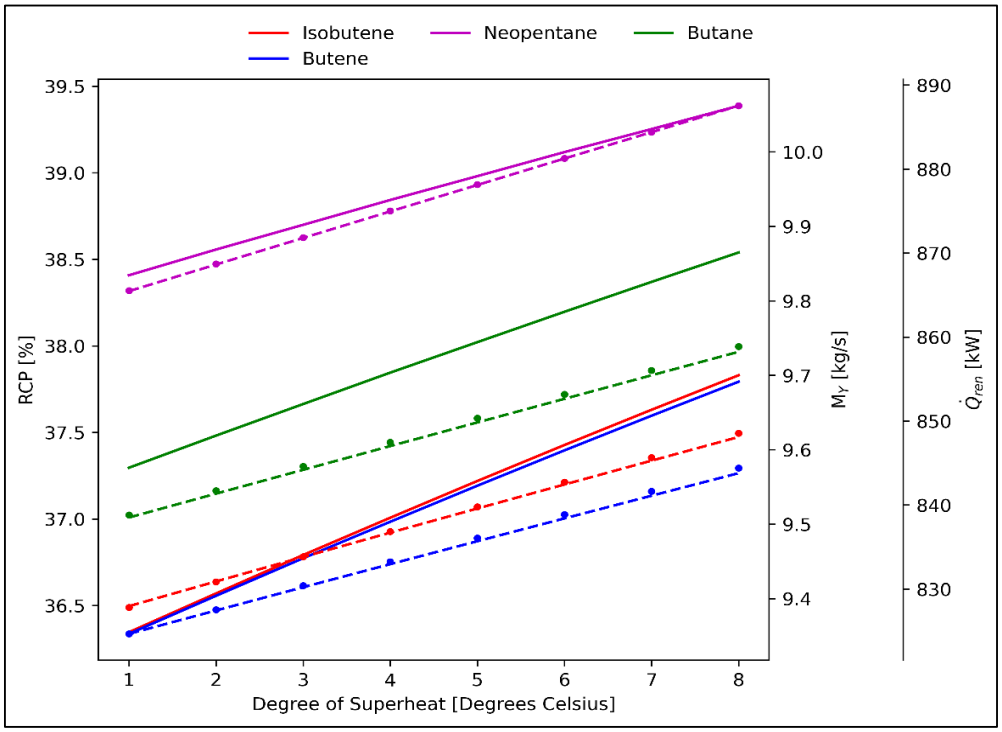


(**a**)

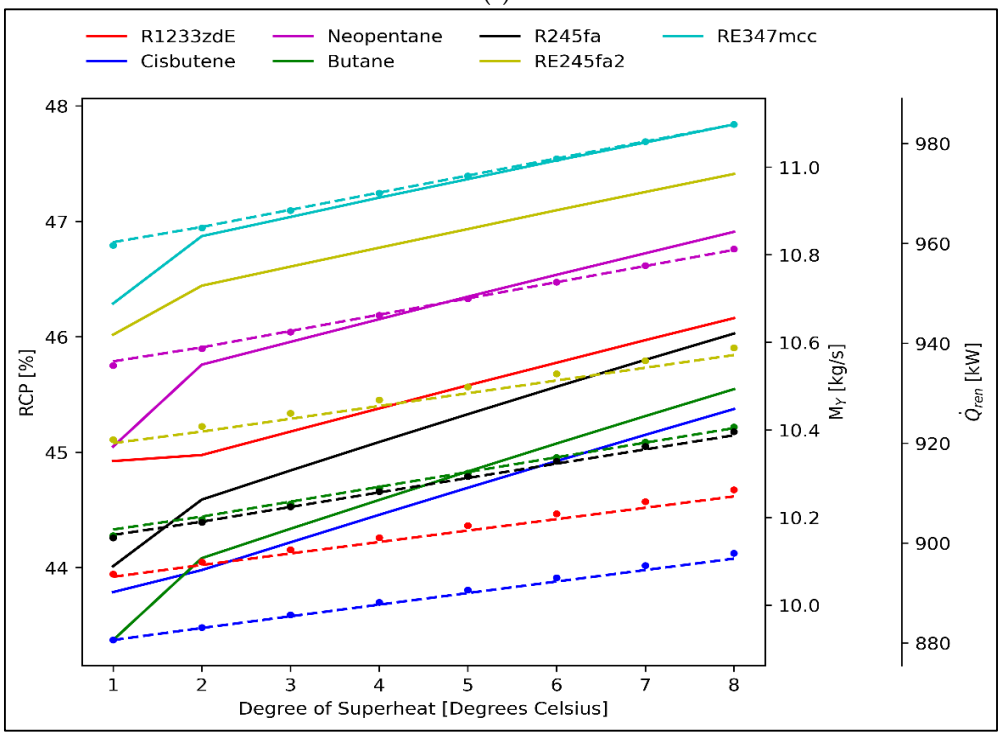


(**b**)

Figure 6. *Cont.*



(**c**)



(**d**)

Figure 6. Degree of evaporator superheat vs. reduction in power consumption and renewable energy input (**a**) at 90 °C; (**b**) at 100 °C; (**c**) at 110 °C; and (**d**) at 120 °C. Solid Lines: *RCP*, Dots: $\dot{Q}_{ren}$, Dashed Lines: M_Y.

At 90 °C, there was a limit to which the superheating could be extended for wet working fluids. It was attributed to the fact that they already exhibit noticeable superheating. This high degree of superheating was necessary to prevent the presence of liquid at the expander outlet. To fulfill the condition of evaporator PPTD, the degree of superheating

range was reduced for the wet working fluids. For the dry/isentropic working fluids, the range started with the baseline value of 1 °C, whereas for the wet working fluids, the range began from (T_2 at baseline + 11 °C; please refer to Figure 3). Moreover, propyne was not depicted in the graph, as the degree of superheating would violate the condition of a minimum of 5 °C PPTD; for propyne, the expander inlet temperature was found to be approximately 95 °C.

As the degree of superheating increased, the RCP increased, but so too did the renewable energy input and the supply water mass flow rate. Regarding the RCP, the reason for its increase with an increase in the degree of superheating was attributed to an increase in the expander work output and the decrease in the pump work input. To explain further, as the degree of superheating increases, the evaporator pressure decreases to meet the pinch point conditions. In doing so, however, the expander inlet enthalpy H_2 increases slightly more than the expander outlet enthalpy H_3. For example, considering isobutene's case at the heating source inlet temperature of 100 °C, the percent increase in the H_2 would be approximately 4%, while for H_3, it would be 3.3%. At the same time, a decrease in evaporator pressure would cause the pump work to decrease. That is, considering the case of isobutene, the percent decrease would be 2.24%. Therefore, with an increase in the expander work output and a decrease in the pump work input, the RCP increases as we increase the degree of superheating.

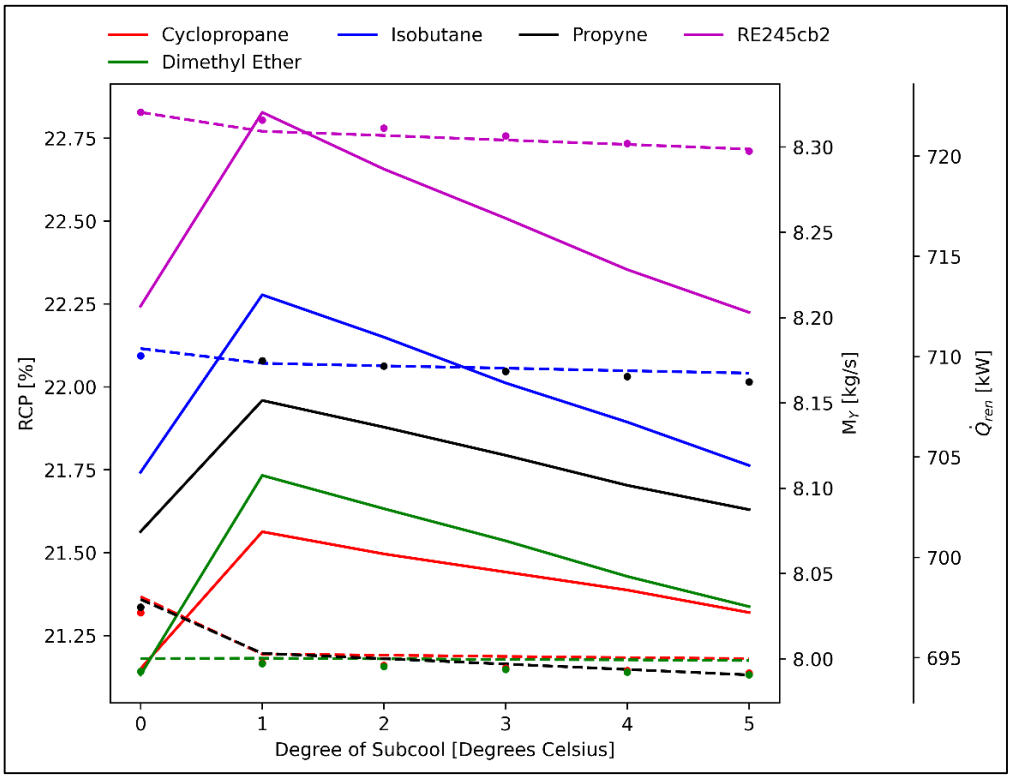
At 90 °C, RE245cb2 displayed the maximum value of *RCP*, which was found to be 22.82%. Similarly, RE245cb2 gave the maximum *RCP* value at 100 °C, approximately at around 31.85%. Meanwhile, at 110 °C and 120 °C, the maximum value of *RCP* was shown by neopentane and RE347mcc, with values of 39.39% and 47.84%, respectively.

The increase in renewable energy, as an increase in the degree of superheating, was due to the decrease in the ORC evaporator pressure. As previously mentioned above, with an increase in the degree of superheating, the ORC evaporator pressure decreases to satisfy the PPTD condition. This decrease in evaporator pressure results in lower values of temperature at state G, the ORC heating source outlet. This, in turn, results in lower values of temperature at state X1″, thereby resulting in a larger renewable energy requirement for raising the temperature to the required amounts at the ORC evaporator heat source inlet. The minimum value of renewable energy input at 90 °C was shown by DME standing at 694.32 kW. Similarly, the minimum values of the $\dot{Q}_{ren}$ at the T_{X2} of 100 °C and 110 °C were shown by butene and at 120 °C by cis-butene. At these temperatures, their respective values were found to be 755 kW, 825 kW, and 880 kW. Meanwhile, the $\dot{Q}_{ren}$ variations ranged from 2.9% for butene to 3.9% for RE245cb2.

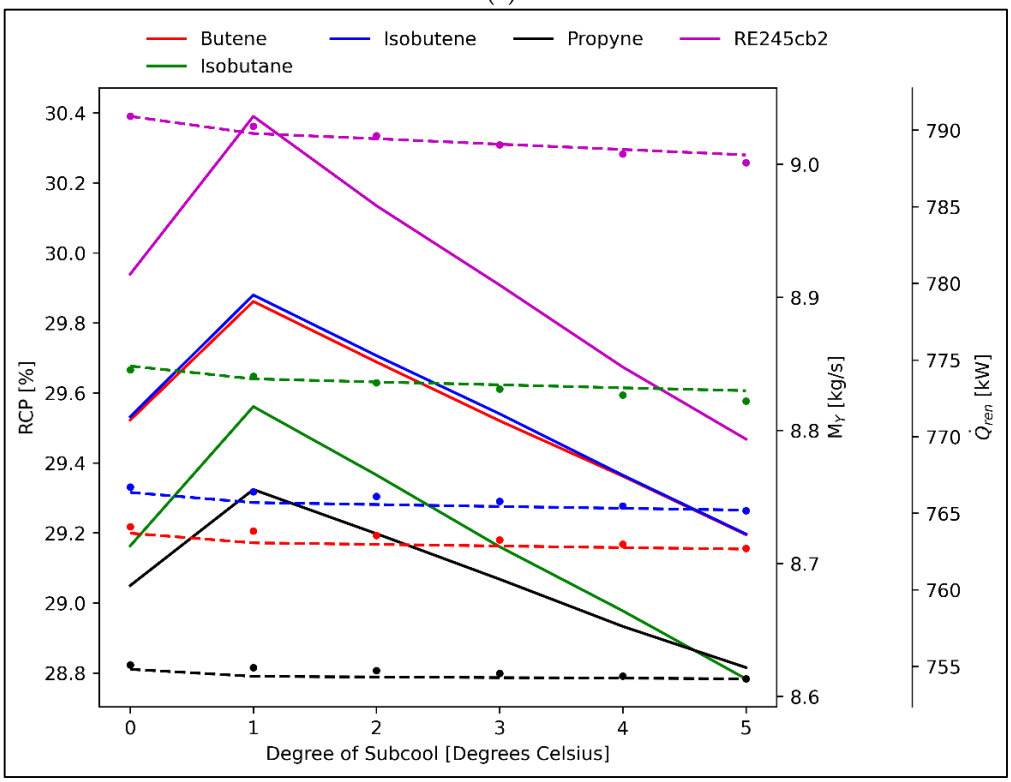
The supply water flow rate, which also increased with an increase in the degree of superheating, showed such behavior because of the decrease in the ORC evaporator with a decrease in the degree of superheating. This is because, as the ORC evaporator decreases with increasing the degree of superheating, the H_3 increases, causing the T_F to increase. For the case of isobutene at heat source inlet temperature of 100 °C, the T_F increases from 45.54 °C to 46.13 °C. This increase in temperature, if we follow the ORC condenser stream colored in blue, causes the T_J to increase slightly, thereby increasing the water supply flow rate.

4.2.2. Effect of ORC Condenser Degree of Subcooling

The effects of increasing the ORC condenser subcooling are portrayed in Figure 7. The trends regarding the RCP and the renewable energy inputs were observed to be more or less similar for all heat source temperatures.

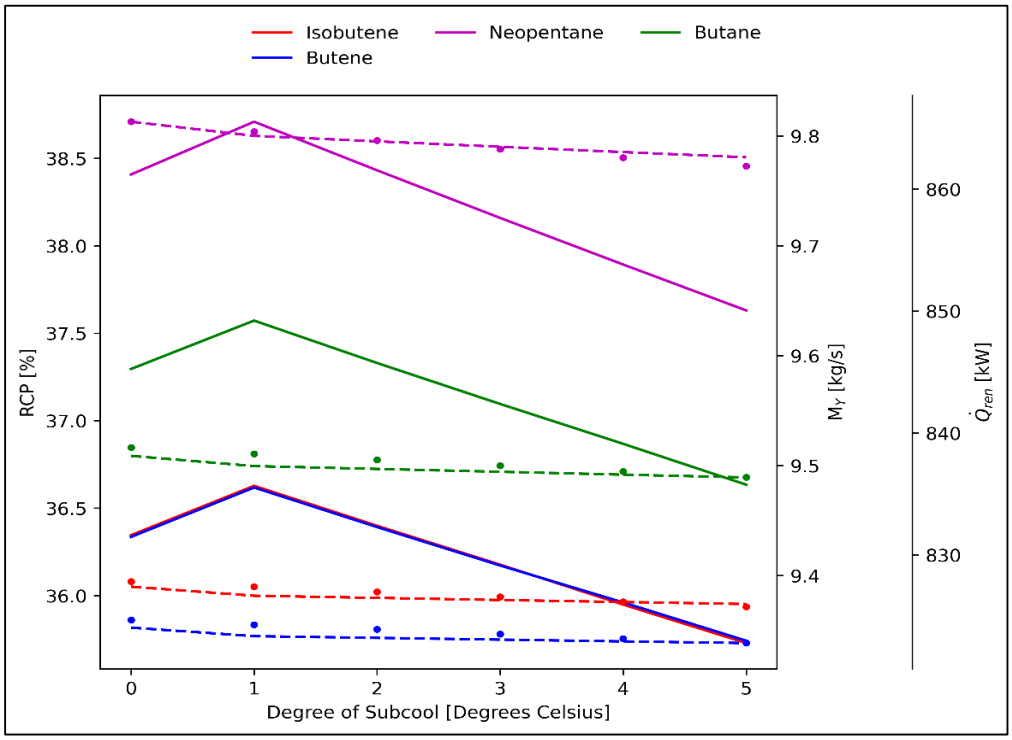


(**a**)

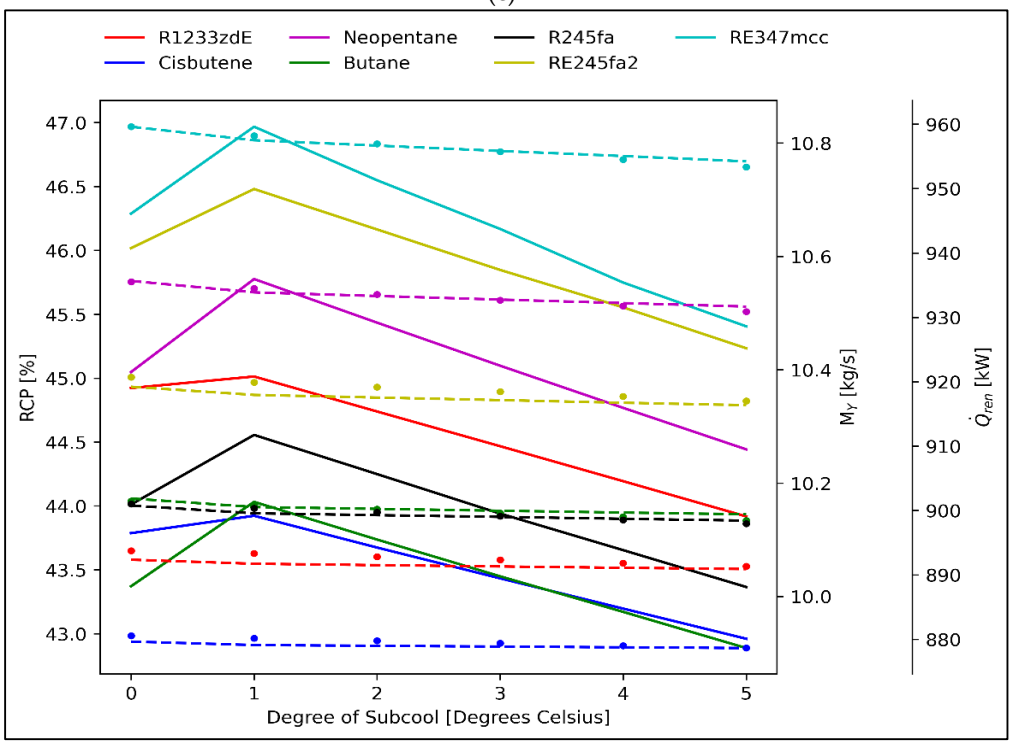


(**b**)

Figure 7. *Cont.*



(**c**)



(**d**)

Figure 7. Degree of condenser subcooling vs. reduction in power consumption and renewable energy input (**a**) at 90 °C; (**b**) at 100 °C; (**c**) at 110 °C; and (**d**) at 120 °C. Solid Lines: *RCP*, Dots: $\dot{Q}_{ren}$, Dashed Lines: M_Y.

Initially, the *RCP* was observed to increase, but afterward its percentage decreased. As the degree of subcooling increased, the expander work output, as well as the work inputs to the ORC pump, decreased. In the case when the subcooling was 1 °C, the pump work decrease was more pronounced compared to the reduction observed in the expander

work output, thereby causing a bump in the trend. To illustrate, consider butene at a T_{X2} of 100 °C, as the degree of subcooling increased from 0 to 1 °C; the decrease in the ORC output would be 0.22 kW. Simultaneously, the decrease in the pump work input as the degree of subcooling increased from 0 to 1 °C would be 0.578 kW. At higher values of subcooling, however, the decrease in the expander work output would start to catch up with the decrease in the power consumption of the pump, thereby causing the RCP to decrease. That is, as the degree of subcooling increases from 1 to 2 °C, the decrease in the $\dot{W}_{EXP}$ would be 0.19 kW, whereas the decrease in the $\dot{W}_{PUMP}$ would be 0.012 kW. Therefore, at higher values of degrees of subcooling, the RCP decreases because of the slightly more rapid decrease of the expander work output in comparison with the pump work decrease. The working fluids isobutane, RE245cb2, neopentane, and RE347mcc had the best performance at the ORC evaporator inlet temperatures of 90 °C, 100 °C, 110 °C, and 120 °C, respectively.

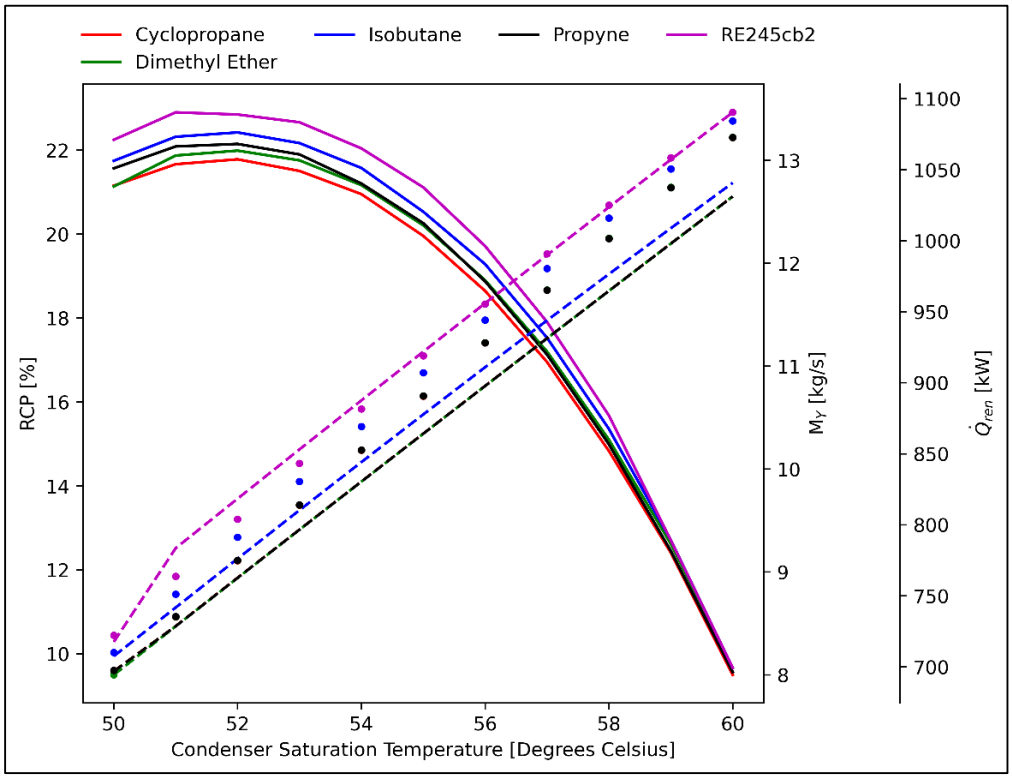
In the case of renewable energy inputs and the supply water, the trends were similar, and they decreased with an increase in the degree of subcooling, but their decrease was observed to be relatively less pronounced.

4.2.3. Effect of ORC Condenser Saturation Temperature

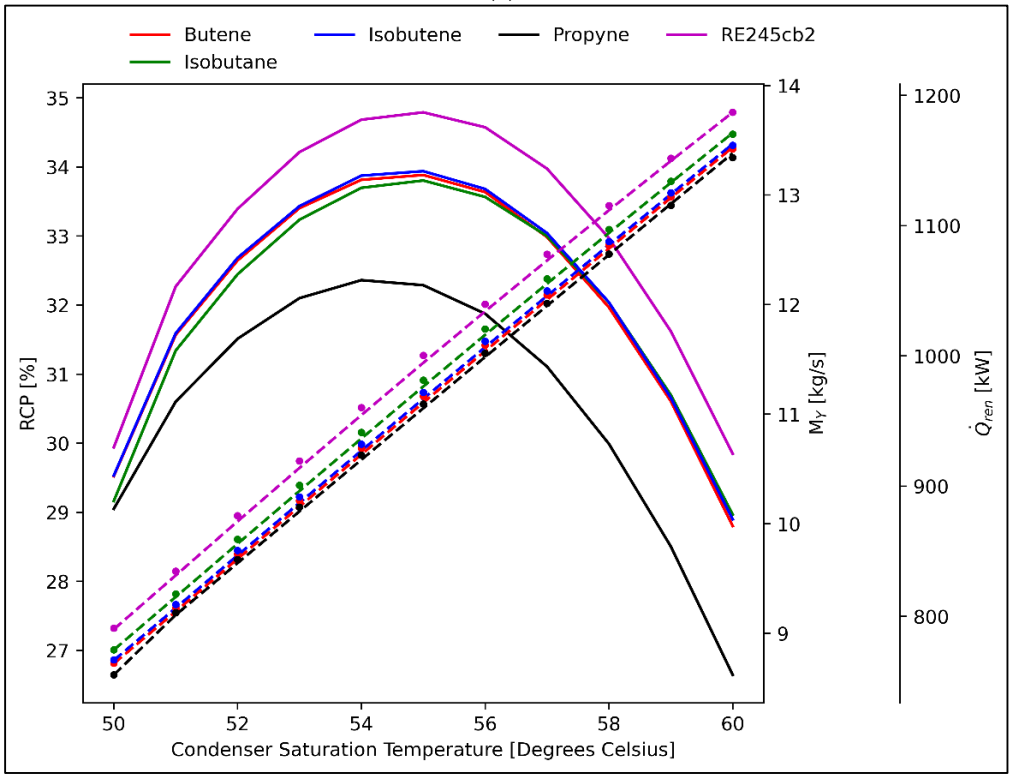
The trends of the *RCP* and the renewable energy input, concerning condenser saturation temperature, are presented in Figure 8. As the condenser saturation temperature increased, the *RCP* increased until a maximum value, and then reduced sharply for all except the ORC heating source inlet temperature of 120 °C. The optimum values of the *RCP* at the heat source ORC inlet temperatures of 90 °, 100 °C, and 110 °C were found to be at the ORC condenser saturation temperatures of 52 °C, 55 °C, and 58 °C, respectively. To understand the reason for the existence of an optimum value for the *RCP* for the T_{X2} values of 90 °C, 100 °C, and 110 °C, consider the case of butene at the T_{X2} value of 100 °C. Keeping the condenser PPTD value fixed at 5 °C, the ORC cooling source outlet temperature would increase from 45.47 °C to 55.44 °C, as the ORC condenser saturation temperature is increased from 50 °C to 60 °C. With the ORC cooling source inlet temperature fixed at 35 °C, the value of heat dissipated by the condenser increases. This increase in heat dissipation, in turn, would increase the ORC mass flow rate from 1.47 kg/s to 3.07 kg/s. In doing so, however, and with the ORC evaporator and PPTD's value kept constant at 5 °C, the ORC evaporator would decrease from 1371.11 kPa to 1106.73 kPa. As the ORC mass flow rate increases and the evaporator pressure decreases, a certain maximum exists for the expander work output, which results in the observed trends for the *RCP* in Figure 8.

Furthermore, as the ORC condenser saturation temperatures increases, the values of the *RCP* for all working fluids get close to each other in the case of T_{X2} of 90 °C. Similarly, when the T_{X2} had a value of 100 °C, the values of isobutene, butene, and isobutane were very close to one another. Meanwhile, the values of the *RCP* for the isobutene and butene were close to one another at the T_{X2} value of 110 °C.

Regarding the renewable energy input, it increases with an increase in the ORC condenser saturation temperature. As the ORC condenser saturation temperature increases, the value of the T_F increases, and that of the T_G decreases. The value of the T_F causes the $T_{X1'}$ to increase, but the decrease in the T_G overtakes and reduces the value of the $T_{X1''}$ significantly. The reduced values of the T_{X2} in comparison to the values at the baseline causes the enhanced requirements of the $\dot{Q}_{ren}$. As the trends are similar for all working fluids, consider the example of butene at the value of T_{X2} of 100 °C: the value of the T_F increases from 45.47 °C to 55.44 °C, and the value of the T_G decreases from 88.85 °C to 78.90 °C. In doing so, the values of the $T_{X1''}$ decrease from 84.41 to 76.35 °C, resulting in the increase of the $\dot{Q}_{ren}$.



(**a**)



(**b**)

Figure 8. *Cont*.

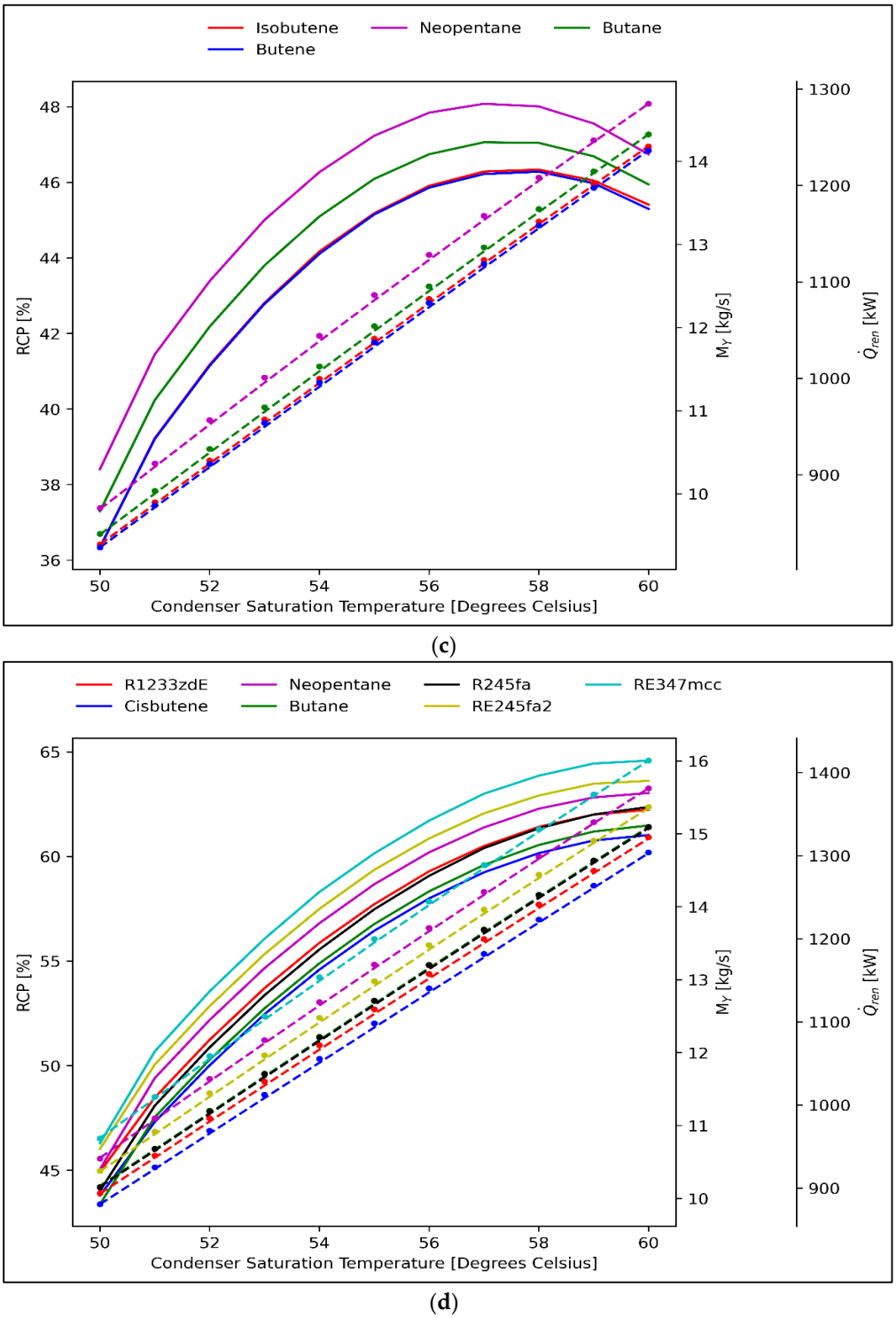


Figure 8. Condenser saturation temperature vs. reduction in power consumption and renewable energy input (**a**) at 90 °C; (**b**) at 100 °C; (**c**) at 110 °C; and (**d**) at 120 °C. Solid Lines: *RCP*, Dots: $\dot{Q}_{ren}$, Dashed Lines: M_Y.

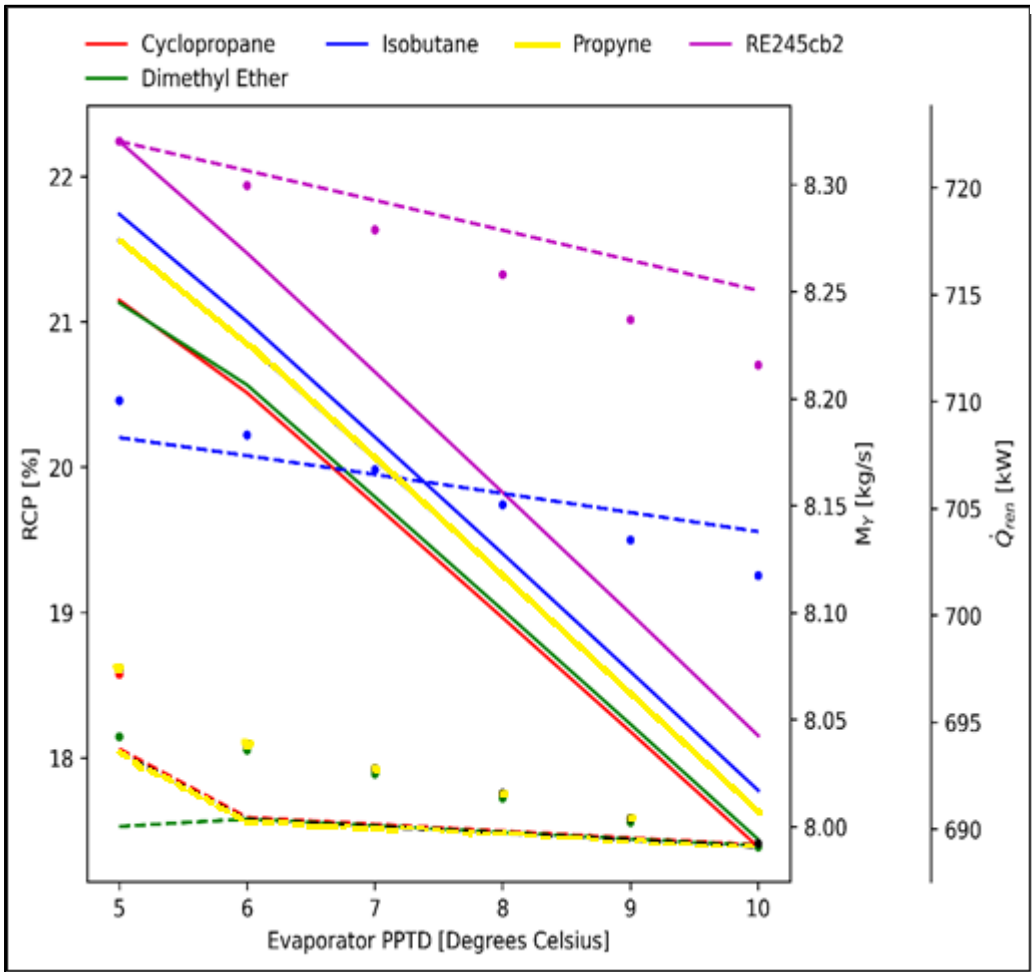
Amongst working fluids, DME, propyne, butene, and cis-butene were found to be the candidates displaying the minimum required renewable energy input at the ORC heating source inlet temperatures of 90 °C, 100 °C, 110 °C, and 120 °C, respectively.

The supply water mass flow rate, M_Y, also increased as the ORC condenser saturation temperature increased. Due to the increase in T_F, the T_I also increased and, at the same

time, keeping in view Equation (11), the decrease in the T_G and $T_{X1''}$ and increase in the $T_{X1'}$, cause the value of the T_J to increase. Therefore, to bring the temperature at state Z to 35 °C, the value of the M_Y increases.

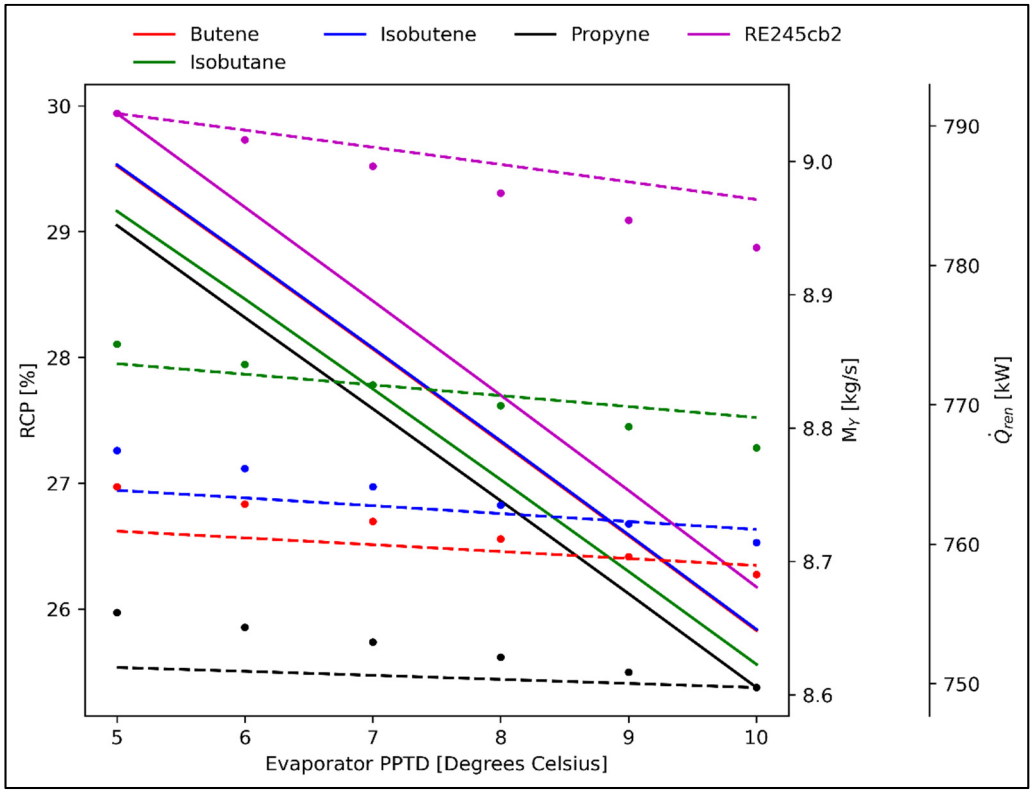
4.2.4. Effect of ORC Evaporator Pinch Point Temperature Difference

The significance of the evaporator PPTD on the reduction of power consumption, renewable energy input, and the supply water mass flowrate is presented in Figure 9. As the evaporator PPTD value increases, the reduction in the power consumption decreases alongside the renewable energy input and the supply water mass flowrate.

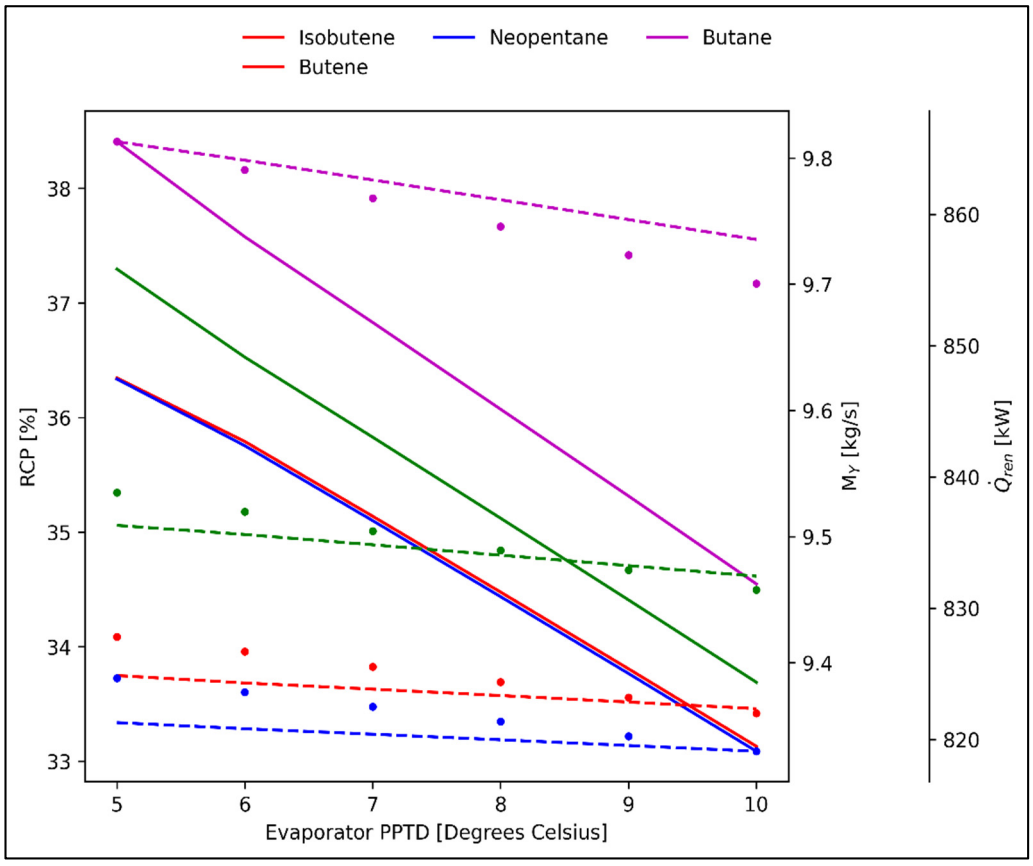


(**a**)

Figure 9. *Cont.*

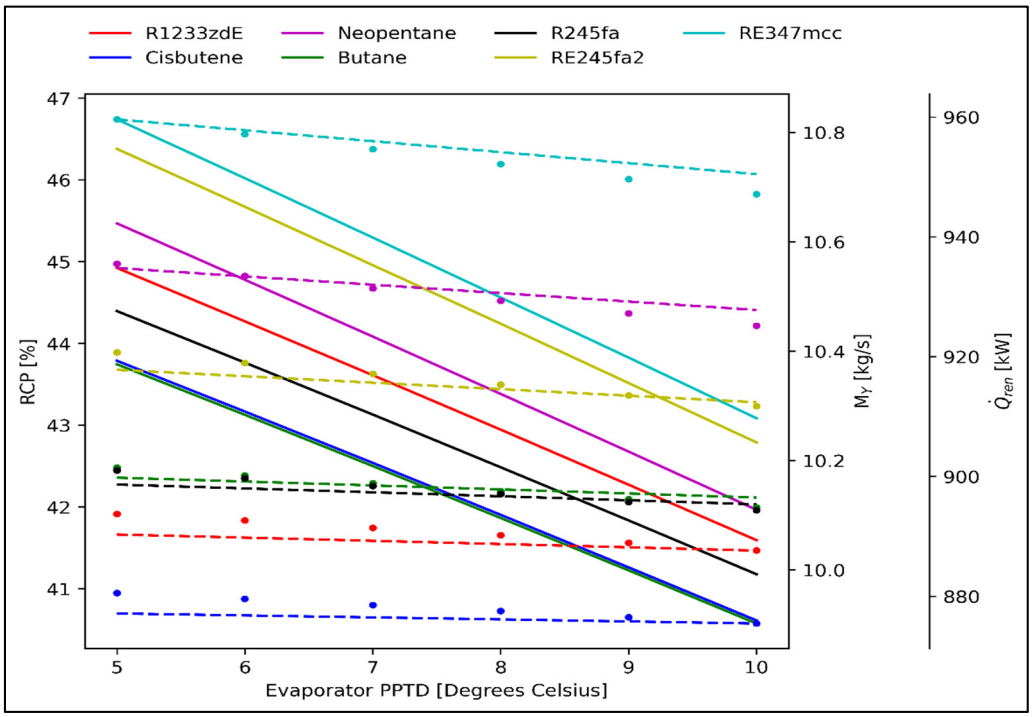


(**b**)



(**c**)

Figure 9. *Cont.*



(**d**)

Figure 9. ORC evaporator pinch point temperature difference vs. reduction in power consumption and renewable energy input (**a**) at 90 °C; (**b**) at 100 °C; (**c**) at 110 °C; and (**d**) at 120 °C. Solid Lines: *RCP*, Dots: $\dot{Q}_{ren}$, Dashed Lines: M_Y.

From the perspective of the *RCP*, it decreased as the evaporator PPTD increased. As the evaporator PPTD increased, the ORC evaporator pressure decreased, thereby decreasing the *RCP* values. The same behavior was observed for all values of T_{X2}. RE245cb2 stood out at the heating source inlet temperatures 90 and 100 °C, whereas neopentane and RE347mcc were the ideal candidates at the heating source inlet temperatures of 110 °C and 120 °C, respectively.

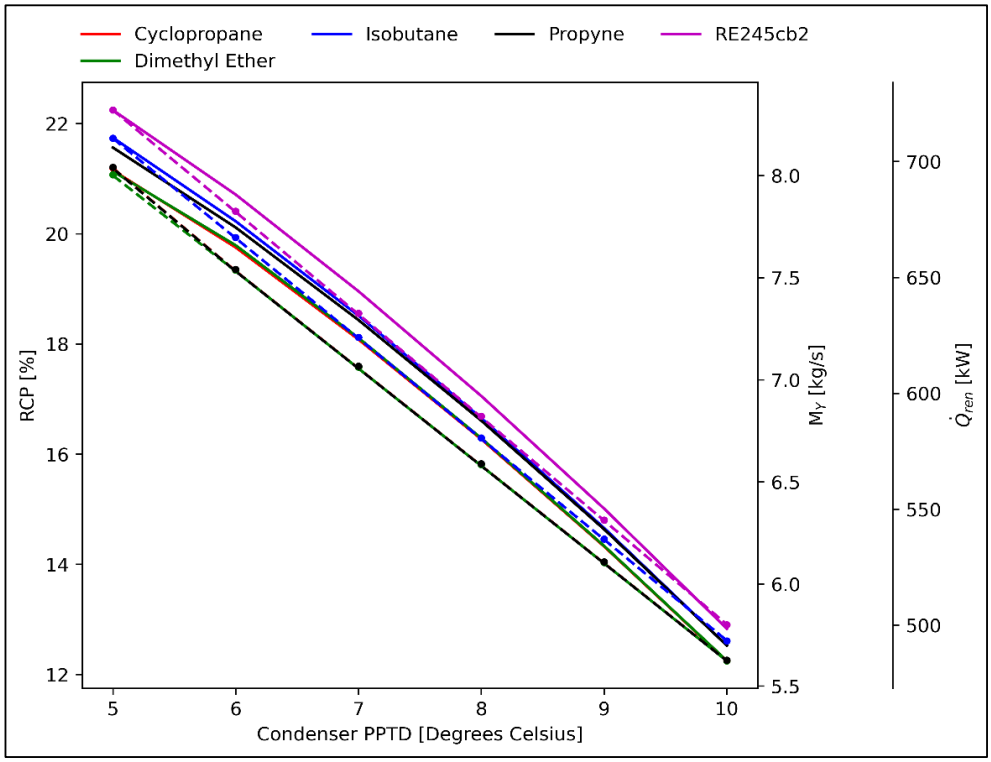
The renewable energy input also decreased in a linear fashion when the ORC evaporator PPTD increased. The reason for this was that, as the evaporator PPTD increased, the value of the T_G increased as well, but only slightly. Due to a slight increase in the value of T_G, the value of $T_{X1''}$ also increased to a limited degree, thereby resulting in a lowering of the $\dot{Q}_{ren}$ requirements. To highlight the magnitude of these changes, consider the example of butene at the T_{X2} value of 100 °C. As the ORC evaporator PPTD increases from 5 °C to 10 °C, the values of T_G would increase from 88.85 to 89 °C, resulting in the increase of the $T_{X1''}$ from 84.41 °C to 84.54 °C, which, in turn, would increases the values of the $\dot{Q}_{ren}$.

The trends remained the same for all the value temperatures of T_{X2}, the ORC heating source inlet temperature. The working fluid with the minimum values of $\dot{Q}_{ren}$ at T_{X2} at 90 °C was DME, with the range of variation from 694 kW to 689 kW, as the PPTD values were raised from 5 °C to 10 °C. At the T_{X2} values of 100°, 110°, and 120 °C, the ideal candidates were found to be propyne, butene, and cis-butene, respectively.

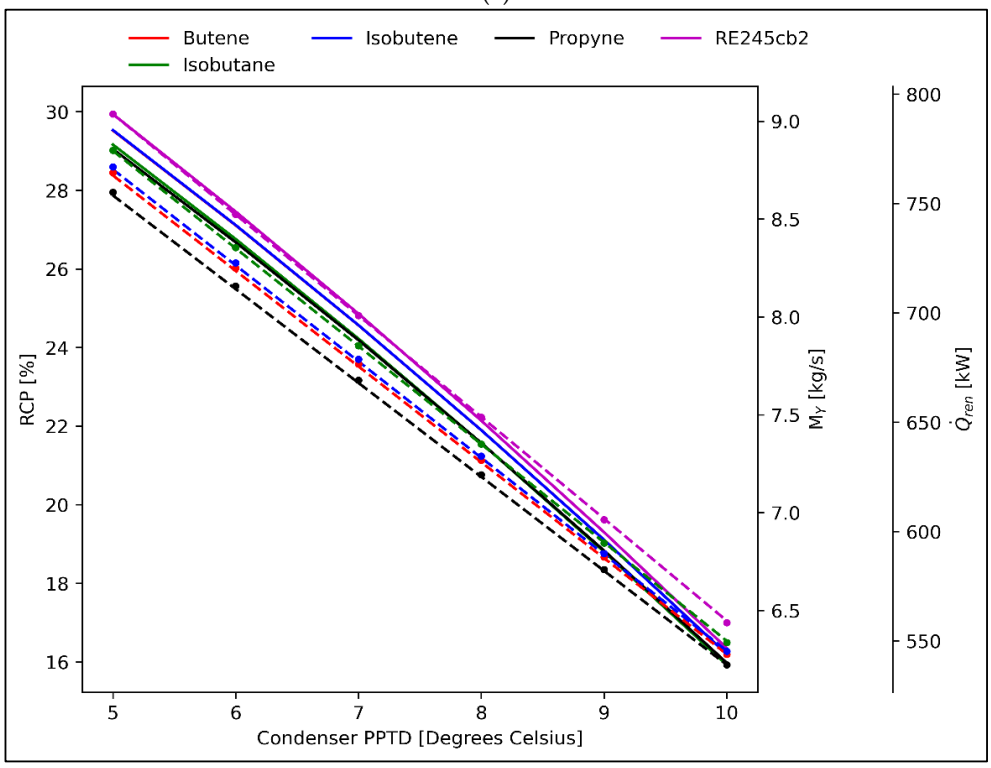
Considering the supply water (M_Y), it also decreased very slightly with an increase in the ORC evaporator PPTD. This was because, as the ORC evaporator PPTD increased, and keeping in view Equation (11), the rise in the T_G, $T_{X1'}$, and $T_{X1''}$ would increase in such a fashion that the T_H would decrease slightly. This slight decrease would cause a slight reduction in the requirement of the supply water intake.

4.2.5. Effect of ORC Condenser Pinch Point Temperature Difference

In this section, the influence of the condenser PPTD on the *RCP*, $\dot{Q}_{ren}$, and M_Y are analyzed, and the results are depicted in Figure 10. The *RCP* and renewable energy input displayed a downward trend.

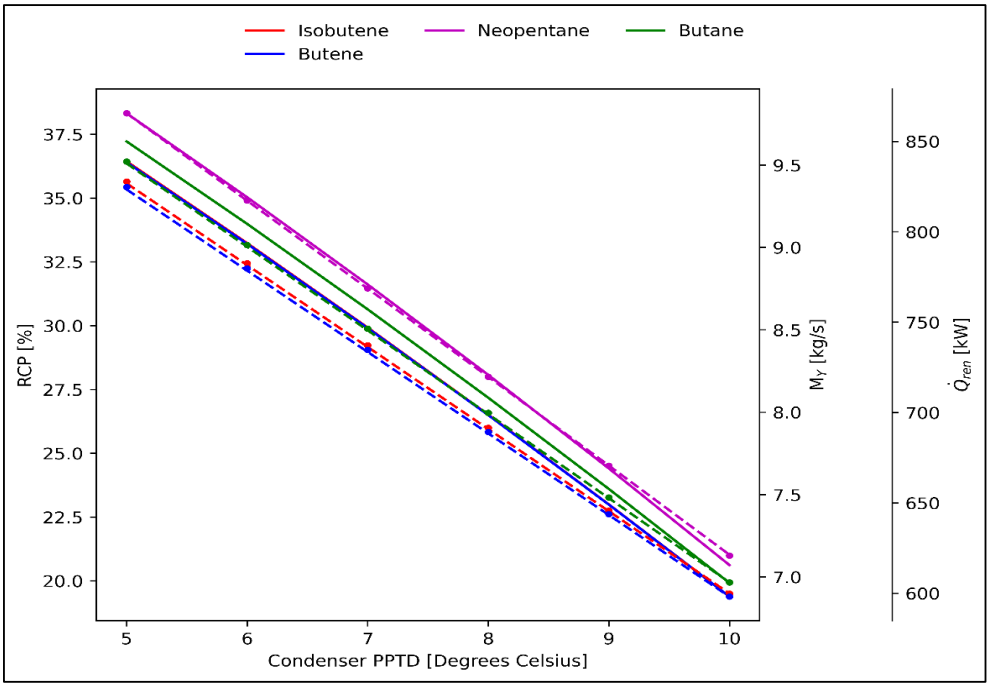


(**a**)

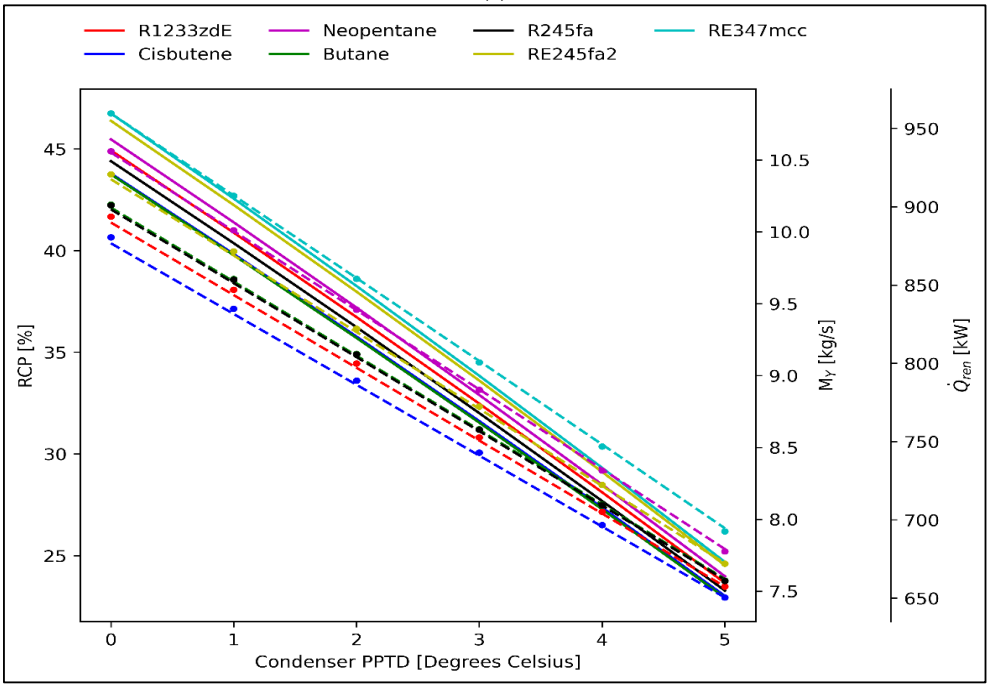


(**b**)

Figure 10. *Cont.*



(**c**)



(**d**)

Figure 10. ORC condenser pinch point temperature difference vs. reduction in power consumption and renewable energy input: (a) 90 °C; (b) at 100 °C; (c) at 110 °C; and (d) at 120 °C. Solid Lines: *RCP*, Dots: $\dot{Q}_{ren}$, Dashed Lines: M_Y.

In this case, as the ORC condenser PPTD increased, the ORC mass flow rate decreased rather drastically. For example, in the case of a T_{X2} with a value of 100 °C and butene, the mass flow rate would decrease from 1.47 kg/s to 0.74 kg/s as the ORC condenser PPTD increased from 5 °C to 10 °C. To understand the decrease in the ORC mass flowrate, keep in mind that the temperature at state B remains constant at 35 °C (the rated VCC condenser outlet temperature; please refer to Table 1). Therefore, as the ORC condenser PPTD increases from 5 °C to 10 °C, the ORC condenser outlet temperature would decrease.

To exemplify this, in the case of butene at T_{X2}, it decreases from 45.48 °C to 40.26 °C. This decrease in the ORC condenser heat dissipation causes the ORC mass flow rate to decline.

With T_{X2} values of 90 °C and 100°C, RE245cb2 gave the maximum values of *RCP*. Meanwhile, at 110 °C and 120 °C, neopentane and RE347mcc presented the highest values of *RCP*, respectively.

The renewable energy input, $\dot{Q}_{ren}$, also decreased with an increase in the condenser PPTD. As previously mentioned above, the T_F decreases with the increase of the ORC condenser PPTD. However, as the ORC mass flowrate falls, the ORC evaporator pressure rises. The increase in the ORC evaporator pressure was attributed to the fulfillment of the ORC evaporator PPTD condition. For example, in the case of butene at the T_{X2} of 100 °C, the ORC evaporator PPTD value increased from 1371 kPa to 1496 kPa. This increase in the ORC evaporator pressure renders an increase in the outlet temperature of the ORC heating source. This temperature, T_G, would increase from 88.85 °C to 94.37 °C for butene at the T_{X2} value of 100 °C. Due to this increase in T_G, the values of $T_{X1''}$ increase consequentially. The amount of renewable energy necessary to raise the temperature of the ORC heating source temperature at the prescribed temperature decreases at the higher values of $T_{X1''}$. DME, propyne, butene, and cis-butene were found to be the ideal candidates at the T_{X2} values of 90 °C, 100 °C, 110 °C, and 120 °C, respectively, with an increase of the ORC condenser PPTD values to 5 °C and 10 °C.

The value of supply water mass flowrate, M_Y, decreased as the value of ORC condenser PPTD was increased. As the ORC condenser PPTD increased, the ORC cooling source outlet temperature decreased, in turn causing the $T_{X1'}$ to fall in accordance with Equation (7). For example, for butene at the T_{X2} value of 100 °C, the value of the $T_{X1'}$ decreased from 44.43 °C to 39.74 °C. At the same time, the values of $T_{X1''}$ increased in accordance with Equation (10), which were dependent on the $T_{X1'}$ and T_G. For butene as ORC working fluid and a T_{X2} value at 100 °C, the $T_{X1''}$ increased from 84.41 °C to 88.91 °C. In between the increase of $T_{X1''}$ and T_G and decrease of $T_{X1'}$, according to Equation (11), the value of T_H would decrease. Again, considering the case of butene as the ORC working fluid with a T_{X2} value of 100 °C, the value of T_H would decrease from 48.87 °C to 45.20 °C as the value of ORC condenser PPTD was increased. The value of T_I remained almost the same as the value of the ORC condenser PPTD increased. Therefore, the temperature of T_J was determined from Equation (13) and was dependent on the temperatures at the states C, H, and I decreasing with an increase in the ORC condenser PPTD. The value of T_J for butene as the ORC working fluid and the value of T_{X2} at 100 °C decreased from 39.98 °C to 38.59 °C. Hence, a smaller amount of supply water was required to keep the temperature of water at state Z to 35 °C.

4.2.6. Effect of ORC Heat and Cold Source Mass Flowrate

The effects of heat and cold source mass flowrate are depicted in Figure 11. At relatively low values of heat and cold source mass flowrates, that is, at (0.1 × 11.67 kg/s) heat source mass flow rate and (0.1 × 11.67 kg/s) cold source flow rate, the outcomes were positive, but limited. At 100 °C, butene displayed a 2.95% *RCP* with a requirement for 76.4 kW of heat from renewable resources. Similarly, at the ORC evaporator inlet temperatures of 120 °C, neopentane displayed a 4.56% RCP with a requirement for 93.55 kW of heat from renewable resources. As the heating source mass flowrate was being raised, however, while keeping the cooling flowrate fixed, the difference between the consecutive values decreased. That is, considering the case of butene with the T_{X2} value of 100 °C, the value of the *RCP* increased from 2.95% at the heating source mass flowrate of (0.1 × 11.67 kg/s) to 3.24% at the heating source mass flow rate of (0.2 × 11.67 kg/s), while the cooling source mass flow rate was kept fixed at (0.1 × 11.67 kg/s). The value of the *RCP* at heating source mass flow rate of (0.3 × 11.67 kg/s) became 3.32%, and at (0.4 × 11.67 kg/s), it became 3.37%. This gap/difference between the *RCP* values continued to decrease as the heating source mass flowrate was increased, while maintaining a fixed cooling source mass flowrate. The same trend was observed for all working fluids for at all values of T_{X2}. At the higher values of

cooling source mass flowrate and lower values of heating source mass flowrate, the ORC system failed to operate due to a lack of available heat.

From the perspective of renewable energy inputs, lower heat source flow rates would require less energy input to raise its temperature, set for the ORC evaporator input. The trend of its increase was linear for all working fluids when the condenser cooling mass flowrate was kept constant and the heating source mass flowrate was increased. Similarly, the same trends were displayed for the supply temperature mass flowrate.

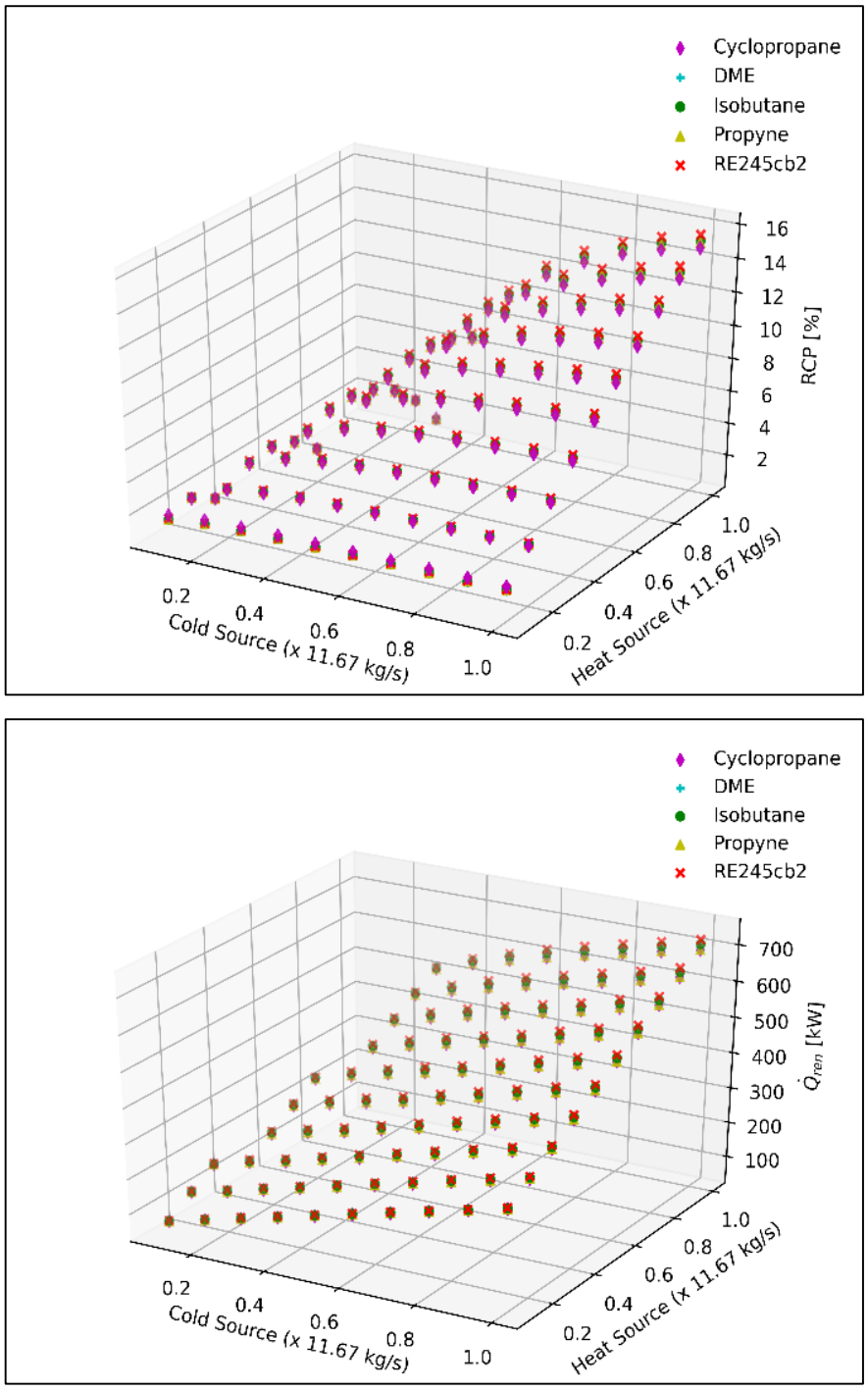
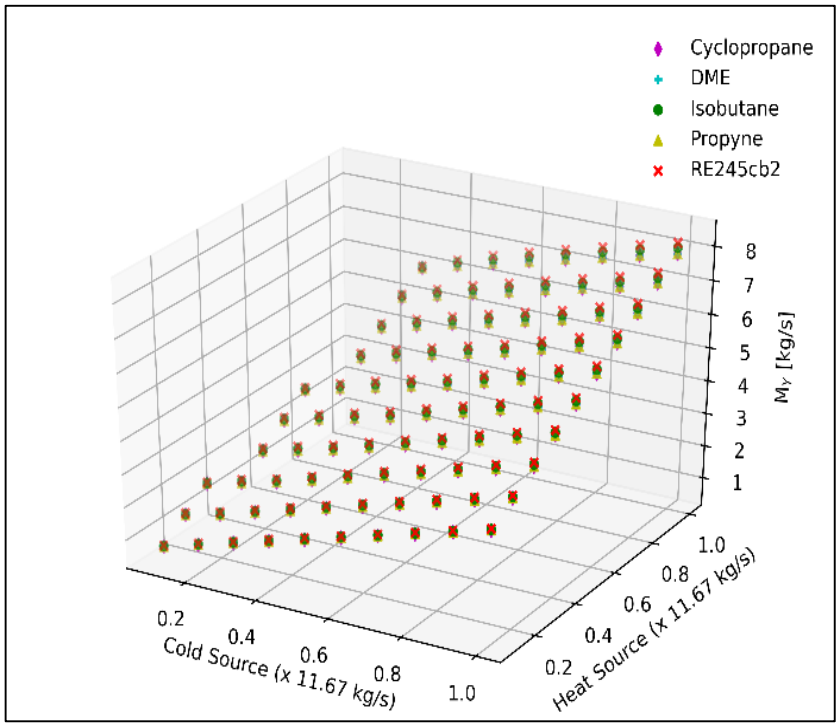


Figure 11. *Cont.*



(**a**)

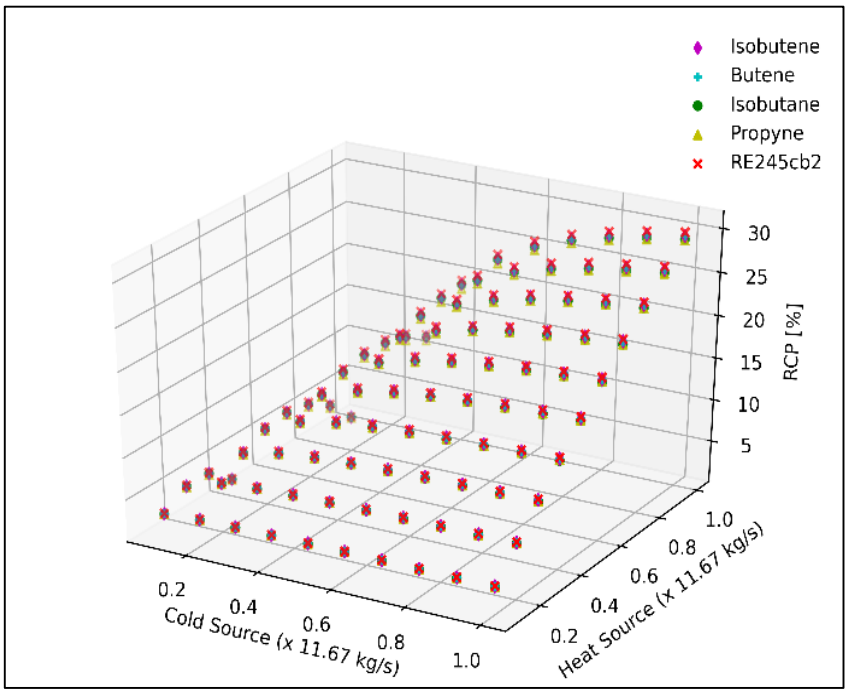
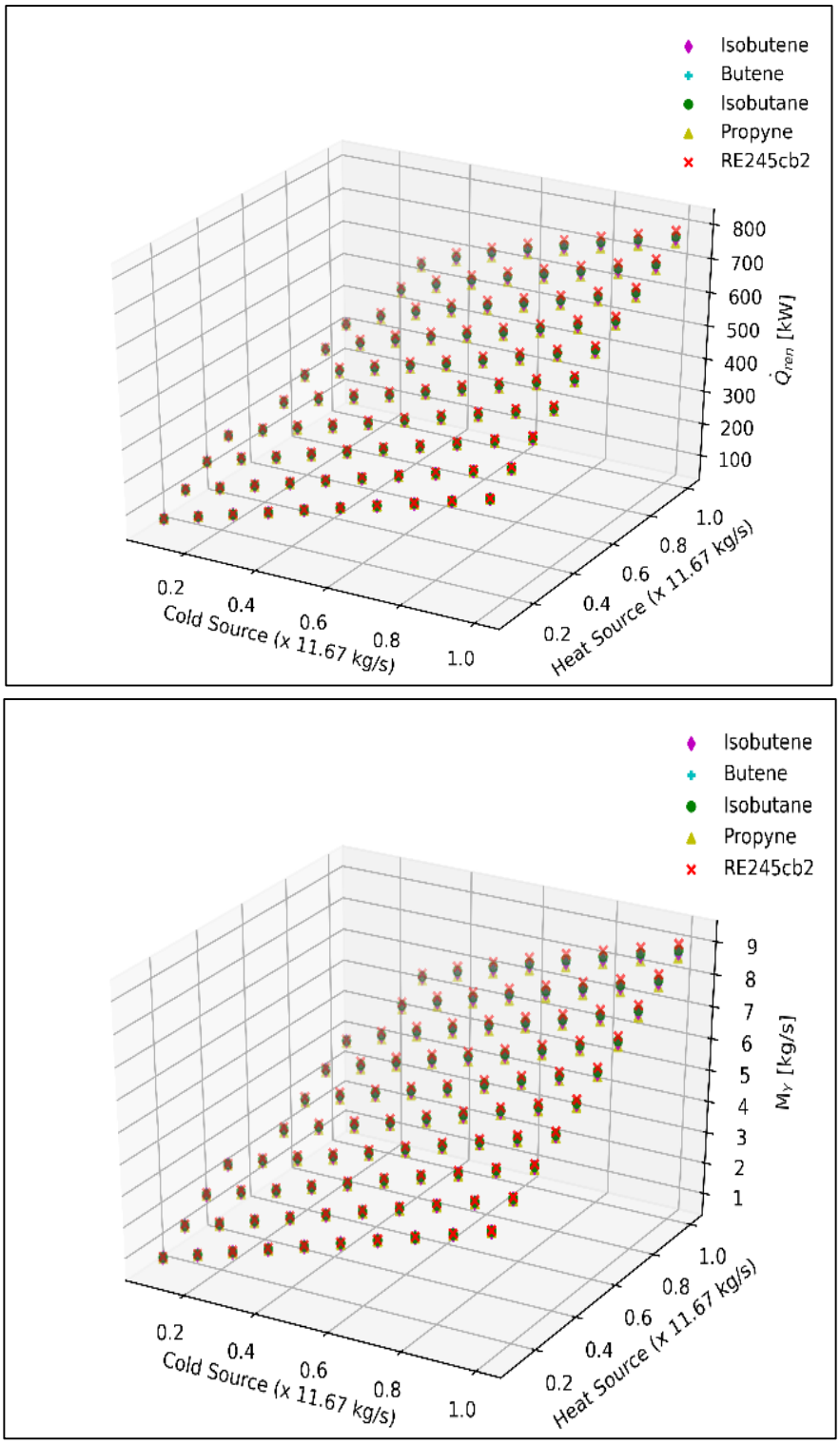


Figure 11. *Cont.*



(**b**)

Figure 11. *Cont.*

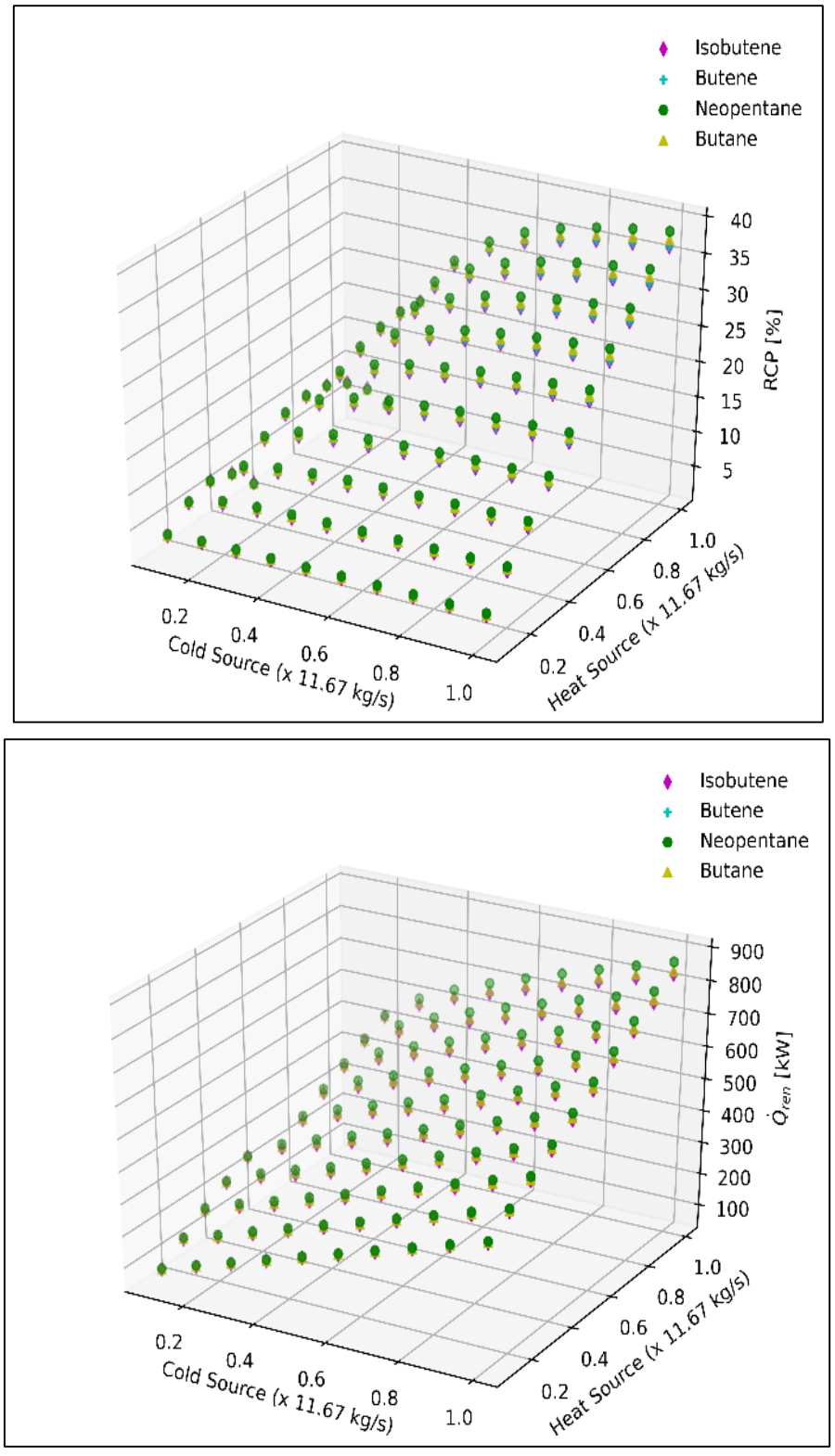
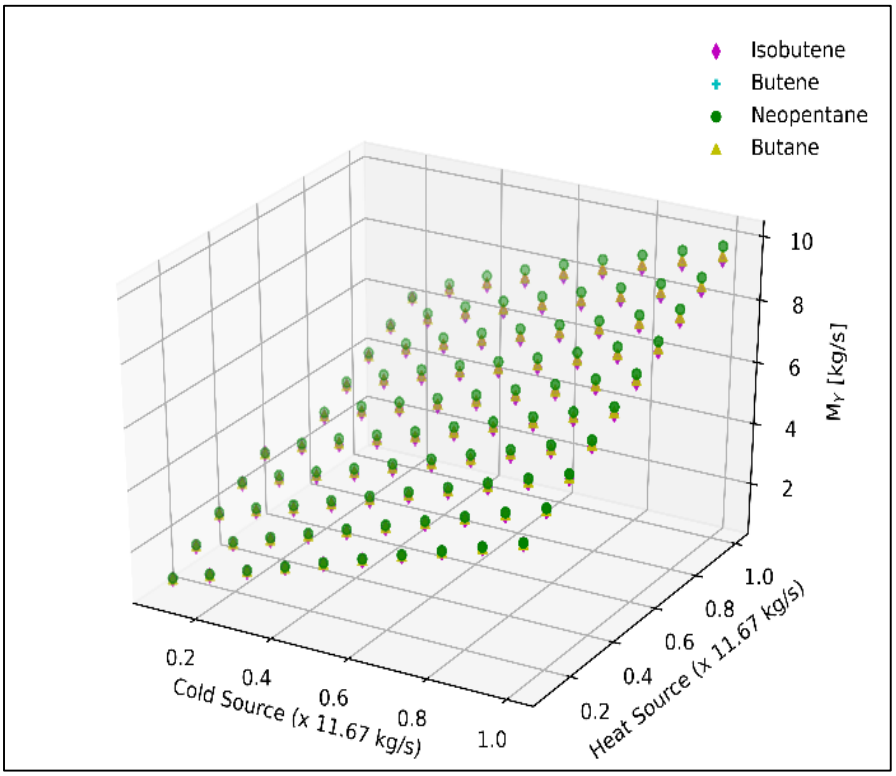


Figure 11. *Cont.*



(**c**)

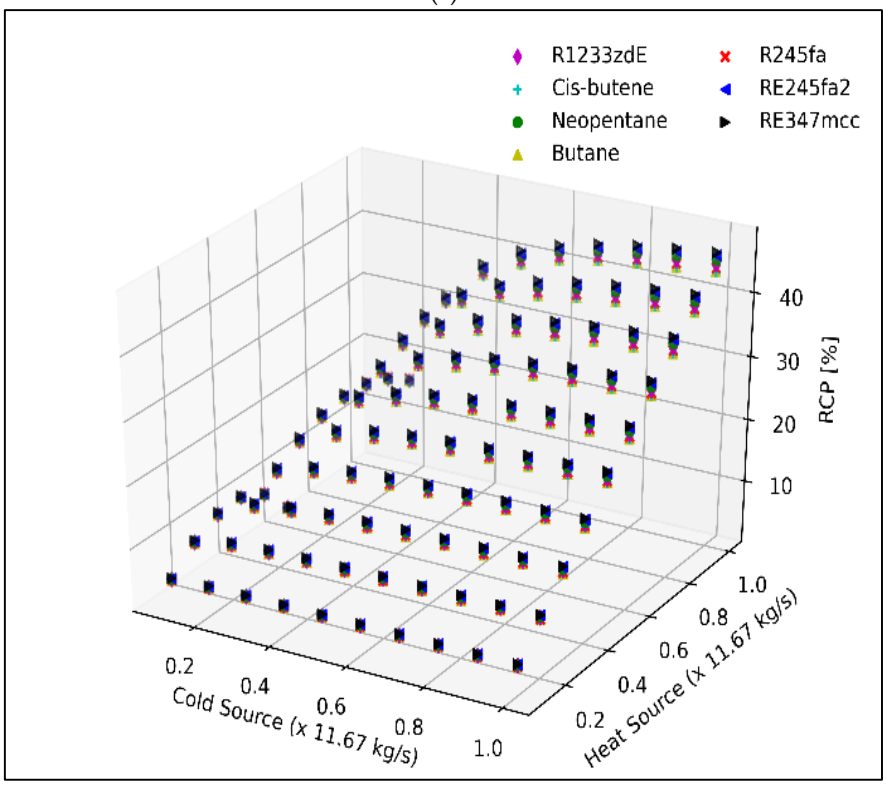
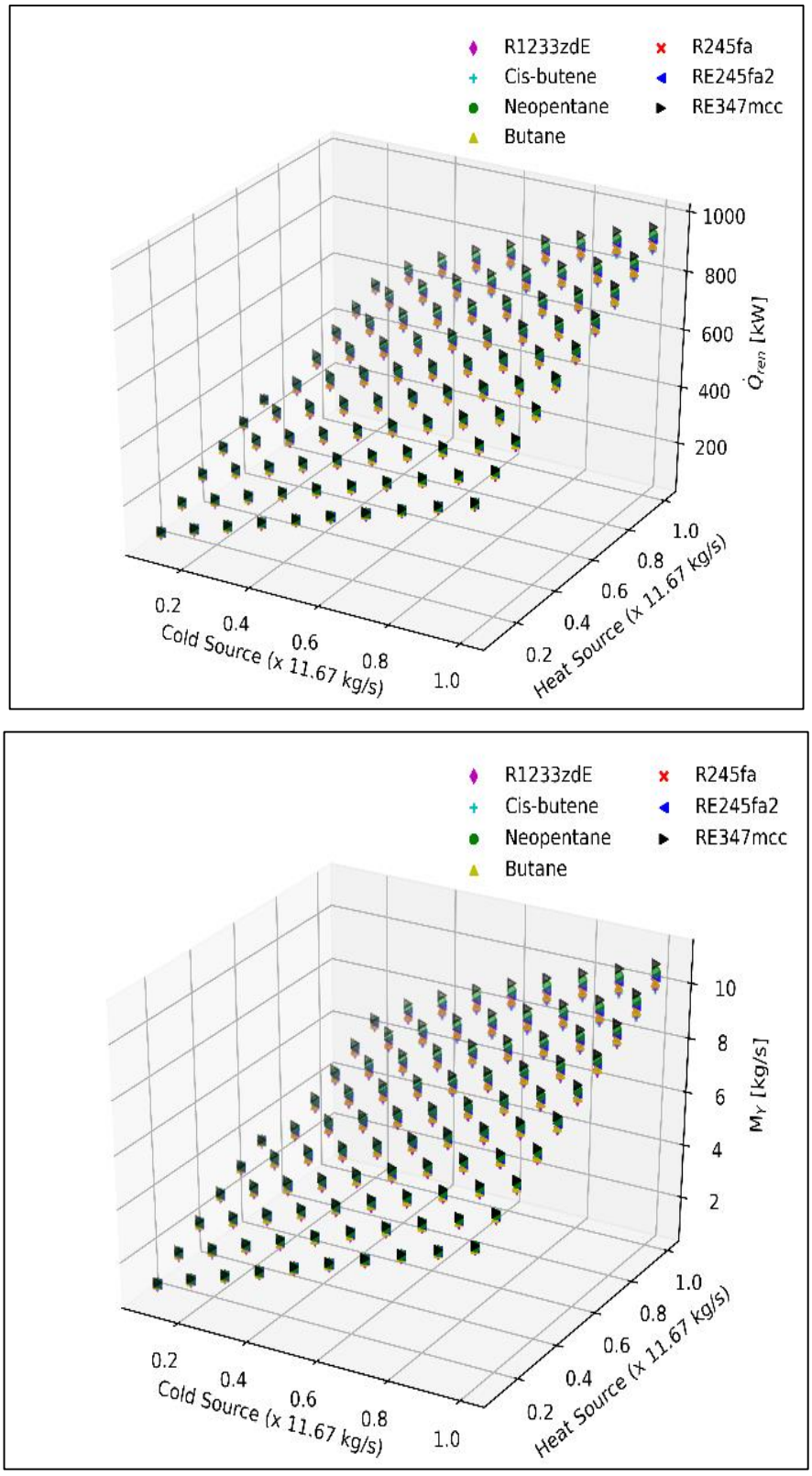


Figure 11. *Cont.*



(**d**)

Figure 11. Heat source mass flowrate and cold source mass flowrate vs. *RCP*, $\dot{Q}_{ren}$, and M_Y (**a**) at 90 °C, (**b**) at 100 °C, (**c**) at 110 °C, and (**d**) at 120 °C.

4.2.7. Optimization

Owing to the non-linear and interdependent nature of the thermal equations, the global optimal solution was determined using the genetic algorithm. The genetic algorithm has been used extensively in the past to find the global optimized values for the thermal systems, as can be found in refs. [58–64]. The parameters to perform the optimization were adopted from Imran et al. [65] and are mentioned below in Table 8.

Table 8. Parameters of genetic algorithm.

Genetic Algorithm Parameter	Values
Size of population	100
Objective function tolerance	0.001
Crossover fraction	0.7
Mutation fraction	0.06
Selection process	Tournament

The objective function, given below, was optimized (maximized):

$$f = \frac{\dot{W}_{EXP} - \dot{W}_{PUMP}}{\dot{Q}_{ren}} \quad (17)$$

As the values of the M_Y were found to be very close to each other for each working fluid it, was neglected. Apart from this, since the hot and cold mass flowrates for each of the working fluids were found to be indifferent to the working fluid, it was also ignored. The range of the parameters were adopted from Table 5, with the exception of the evaporator superheat, which was adopted accordingly from Figure 6. The results are presented in Table 9.

Table 9. Optimization results.

Heat Source Temperature (°C)	Working Fluid	Condenser Saturation Temperature (°C)	Degree of Sub Cool (°C)	Condenser Pinch Point Temperature Difference °C)	Degree of Superheating (°C)	Evaporator Pinch Point Temperature Difference (°C)	Equation (17) (%)
90	DME	50	0.01	5	4.91	5	4.58
	Cyclopropane	50	0.17	5	3.99	5	4.28
	Propyne	50	0.0	5	2.96	5	4.03
	Isobutane	50	0.39	5	1	5	3.26
	RE245cb2	50	0.55	5	1.35	5	3.26
100	Butene	50.1	0.75	5.05	9.63	5	4.13
	Isobutene	50	0	5	9.94	5	4.11
	Propyne	50	0.11	5	0.0	5	4.07
	Isobutane	50	0.62	5	9.53	5	4.02
	RE245cb2	50	0.05	5	4.60	5	4.00
110	Butene	51.50	0.42	5	9.26	5	4.75
	Butane	50.84	0.55	5.07	9.71	5	4.75
	Isobutene	50.68	0.29	5	9.99	5	4.74
	Neopentane	51.19	0.57	5	2.32	5	4.70
120	R1233zd (E)	53.04	0.52	5.01	9.93	5.03	5.47
	Cis-butene	52.73	0.56	5	9.88	5	5.47
	RE245fa2	52.50	0	5	2.27	5	5.42
	R245fa	52.67	0.76	5.07	9.97	5.24	5.36
	Butane	52.23	0.41	5	9.55	5	5.32
	Neopentane	52.60	0.55	5	1.99	5	5.25
	RE347mcc	52.42	0	5	1	5	5.24

The best working fluids of the ORC were found to be DME and butene for the ORC evaporator inlet temperatures of 90 °C and 100 °C, respectively. Meanwhile, for the ORC evaporator temperatures of 110 and 120°C, the ideal working fluid candidates were found to be butene and R1233zd (E). For DME, at the heat source ORC evaporator inlet temperature of 90 °C, the improvement in the rated COP was found to be 48.72%, at the expense of a renewable energy input of 710 kW and an external water supply of 8.2 kg/s. Meanwhile, at the ORC evaporator inlet temperature of 100 °C, for butene, the improvement in COP was 48.76%, with a renewable energy input at 790 kW and an additional water supply of 9.14 kg/s. At the heat source ORC evaporator inlet temperature of 110 °C, the COP improvement was 68.85% with a renewable energy input requirement of 852 kW and an additional water supply of 9.78 kg/s. For the heat source ORC evaporator inlet temperature of 120 °C, the improvement was 140.88% with a renewable energy input of 1061 kW and an additional water mass flowrate of 12 kg/s.

Further research including possible variations of the recuperators and external water supply, with a focus on the economic and the ecological aspects, are also under consideration for the case study of improving the performance of the existing large scale VCC chillers.

5. Conclusions

This work presented a scheme to reduce the work consumption of an industrial chiller using renewable energy sources and an ORC system. Thermal analysis was conducted considering the ORC evaporator temperatures of 90 to120 °C by a step of 10 °C. Sensitivity analyses considering the degree of superheating, degree of subcooling, condenser saturation temperature, ORC evaporator and condenser PPTDs, and heat source and cold source mass flow rates were conducted. The main findings were categorized as follows:

- As the degree of superheating increased, the VCC input work reduction also increased. The renewable energy input also increased with the degree of superheating. The supply water flowrates also increased with an increase in the degree of superheating.
- When the degree of subcooling increased, there existed a maximum at 1 °C in the case of a VCC input reduction in work consumption, whereas it decreased afterward. Renewable energy input and the supply water flowrate decreased slightly when the degree of subcooling increased.
- As the ORC condenser temperature increased, there existed maxima for the VCC input work reduction when the ORC evaporator inlet temperature was 90 °C, 100 °C, and 110 °C. The renewable energy input and the supply water mass flowrate increased with an increase in the ORC condenser saturation temperature.
- For the ORC condenser and the evaporator PPTDs, the reduction for power consumption decreased as the PPTDs was increased. Renewable energy input, as well as the supply water mass flowrate, reduced with an increase in the condenser and the evaporator PPTDs.
- Considering the heat and cold mass flow rates, the scheme become unfavorable at the extreme low ends. The reduction in the VCC work input increased rapidly initially and then slightly as the heating source mass flowrate was increased, while keeping the cooling source mass flowrate constant. The renewable energy input, as well as the supply water mass flowrate, increased with an increase of the heating source mass flowrate, while keeping the cooling source mass flowrate fixed.
- The ideal working fluid from the considered candidates for the heating source ORC evaporator inlet temperatures of 90 °C was found to be DME. For the temperatures of 100 °C and 110 °C, butene was found to be the ideal working fluid. Meanwhile, for 120 °C, the ideal working fluid was found to be R1233zd (E).

Research was conducted to thermally explore the integration of the ORC technology and available renewable energy resources to improve the performance of already installed VCCs, with existing cooling tower setups.

Author Contributions: M.T.N.: Conceptualization, methodology, validation, formal analysis, writing—original draft. M.C.E.: Methodology, visualization, writing—original draft. J.A.E.: Visualization, formal analysis, writing—review and editing. K.C.K.: Supervision, writing—review and editing, funding acquisition. All authors have read and agreed to the published version of the manuscript.

Funding: This research received no external funding.

Institutional Review Board Statement: Not applicable.

Informed Consent Statement: Not applicable.

Data Availability Statement: Data is contained within the article.

Acknowledgments: This work was supported by the National Research Foundation of Korea (NRF) grant, which is funded by the Korean government (MSIT) (No. 2020R1A5A8018822). This work was also supported by Brain Pool Program through the National Research Foundation of Korea (NRF) funded by the Ministry of Science and ICT (NRF-2020H1D3A2A01104062).

Conflicts of Interest: The authors declare no conflict of interest.

Abbreviations

c_P	Specific heat, kJ/kg.K
COP	Coefficient of Performance
H	Specific Enthalpy, kJ/kg
HVAC	Heating, Ventillaitng, and Air Conditioning
$\dot{m}$	Mass flowrate, kg/s
ORC	Organic Rankine Cycle
PPTD	Pinch Point Temperature Difference. °C
$\dot{Q}$	Heat transfer rate, kW
RC	Rated Conditions
RCP	Reduction in Power Consumption
T	Temperature, °C
$\dot{V}$	Volumetric flowrate, m_3/s
VCC	Vapor Compression Cycle
$\dot{W}$	Work transfer, kW
Subscripts:	
1, 2, 3, 4	State point of ORC
A, B, C, F, G, H, I, J, K, X1, X1′, X1″, X2	State Points on the Cooling Circuit of Vapor Compression Chiller
AIR	Air Through Cooling Tower
BOIL	Boiler/Evaporator
COND	Condenser
COMP	Compressor
EXP	Expander
HX	Heat Exchanger
min	Minimum
ORC	Organic Rankine Cycle
PUMP	Pump of Organic Rankine Cycle
η	Second law efficiency
ρ	Density, kg/m^3

References

1. Kumar, Y.A.; Kumar, K.D.; Kim, H. Reagents assisted $ZnCo_2O_4$ nanomaterial for supercapacitor applications. *Electrochim. Acta* **2020**, *330*, 135261. [CrossRef]
2. Pallavolu, M.R.; Nallapureddy, J.; Nallapureddy, R.R.; Neelima, G.; Yellduri, A.K.; Mandal, T.K.; Pejjai, B.; Joo, S.W. Self-assembled and highly faceted growth of Mo and V doped ZnO nanoflowers for high-performance supercapacitors. *J. Alloys Compd.* **2021**, *886*, 161234. [CrossRef]
3. The Paris Agreement. United Nations Climate Change. Available online: https://unfccc.int/process-and-meetings/the-paris-agreement/the-paris-agreement (accessed on 11 August 2021).

4. Li, C.; Zhou, J.; Cao, Y.; Zhong, J.; Liu, Y.; Kang, C.; Tan, Y. Interaction between urban microclimate and electric air-conditioning energy consumption during high temperature season. *Appl. Energy* **2014**, *117*, 149–156. [CrossRef]
5. Henley, J. World Set to Use More Energy for Cooling than Heating. *The Guardian*, 26 October 2015. Available online: https://www.theguardian.com/environment/2015/oct/26/cold-economy-cop21-global-warming-carbon-emissions (accessed on 11 August 2021).
6. Ürge-Vorsatz, D.; Cabeza, L.F.; Serrano, S.; Barreneche, C.; Petrichenko, K. Heating and cooling energy trends and drivers in buildings. *Renew. Sustain. Energy Rev.* **2015**, *41*, 85–98. [CrossRef]
7. Chan, C.; Ling-Chin, J.; Roskilly, A.P. A review of chemical heat pumps, thermodynamic cycles and thermal energy storage technologies for low grade heat utilisation. *Appl. Therm. Eng.* **2013**, *50*, 1257–1273. [CrossRef]
8. Chua, K.J.; Chou, S.; Yang, W.; Yan, J. Achieving better energy-efficient air conditioning—A review of technologies and strategies. *Appl. Energy* **2013**, *104*, 87–104. [CrossRef]
9. Brown, J.S.; Domanski, P. Review of alternative cooling technologies. *Appl. Therm. Eng.* **2014**, *64*, 252–262. [CrossRef]
10. Mardiana-Idayu, A.; Riffat, S. Review on heat recovery technologies for building applications. *Renew. Sustain. Energy Rev.* **2012**, *16*, 1241–1255. [CrossRef]
11. Cuce, P.M.; Riffat, S. A comprehensive review of heat recovery systems for building applications. *Renew. Sustain. Energy Rev.* **2015**, *47*, 665–682. [CrossRef]
12. Minh, N.Q.; Hewitt, N.J.; Eames, P.C. Improved Vapour Compression Refrigeration Cycles: Literature Review and Their Application to Heat Pumps. In Proceedings of the 11th International Refrigeration and Air Conditioning Conference, West Lafayette, IN, USA, 17–20 July 2006. Available online: https://www.osti.gov/servlets/purl/850491 (accessed on 11 August 2021).
13. Seyam, S. Types of HVAC Systems. In *HVAC System*; IntechOpen: London, UK, 2018; pp. 49–66. [CrossRef]
14. Gong, G.; Zeng, W.; Wang, L.; Wu, C. A new heat recovery technique for air-conditioning/heat-pump system. *Appl. Therm. Eng.* **2008**, *28*, 2360–2370. [CrossRef]
15. Sivaram, A.R.; Karuppasamy, K.; Rajavel, R.; Prasad, B.A. Experimental Investigations on the Performance of a Water Heater Using Waste Heat from an Air Conditioning System. *Indian J. Sci. Technol.* **2015**, *8*. [CrossRef]
16. Su, H.; Gong, G.; Zhang, Y. Inversion Method for Optimizing the Condensing Heat Recovery System of an Air-Source Heat Pump. *J. Energy Eng.* **2017**, *143*, 04016069. [CrossRef]
17. Jiang, M.L.; Wu, J.Y.; Xu, Y.X.; Wang, R.Z. Transient characteristics and performance analysis of a vapor compression air conditioning system with condensing heat recovery. *Energy Build.* **2010**, *42*, 2251–2257. [CrossRef]
18. Naldi, C.; Zanchini, E. Dynamic simulation during summer of a reversible multi-function heat pump with condensation-heat recovery. *Appl. Therm. Eng.* **2017**, *116*, 126–133. [CrossRef]
19. Kairouani, L.; Nehdi, E. Cooling performance and energy saving of a compression–absorption refrigeration system assisted by geothermal energy. *Appl. Therm. Eng.* **2006**, *26*, 288–294. [CrossRef]
20. Cimsit, C.; Ozturk, I.T. Analysis of compression–absorption cascade refrigeration cycles. *Appl. Therm. Eng.* **2012**, *40*, 311–317. [CrossRef]
21. Garimella, S.; Brown, A.M.; Nagavarapu, A.K. Waste heat driven absorption/vapor-compression cascade refrigeration system for megawatt scale, high-flux, low-temperature cooling. *Int. J. Refrig.* **2011**, *34*, 1776–1785. [CrossRef]
22. Lemmon, E.W.; Huber, M.L.; McLinden, M.O. *NIST Standard Reference Database 23: Reference Fluid Thermodynamic and Transport Properties-REFPROP*; Version 9.1; NIST Publications: Gaithersburg, MD, USA, 2013.
23. Rahbar, K.; Mahmoud, S.; Al-Dadah, R.K.; Moazami, N.; Mirhadizadeh, S.A. Review of organic Rankine cycle for small-scale applications. *Energy Convers. Manag.* **2016**, *134*, 135–155. [CrossRef]
24. Colonna, P.; Casati, E.; Trapp, C.; Mathijssen, T.; Larjola, J.; Turunen-Saaresti, T.; Uusitalo, A. Organic Rankine Cycle Power Systems: From the Concept to Current Technology, Applications, and an Outlook to the Future. *J. Eng. Gas Turbines Power* **2015**, *137*, 100801. [CrossRef]
25. Martinez, S.; Michaux, G.; Salagnac, P.; Bouvier, J.-L. Micro-combined heat and power systems (micro-CHP) based on renewable energy sources. *Energy Convers. Manag.* **2017**, *154*, 262–285. [CrossRef]
26. Park, B.-S.; Usman, M.; Imran, M.; Pesyridis, A. Review of Organic Rankine Cycle experimental data trends. *Energy Convers. Manag.* **2018**, *173*, 679–691. [CrossRef]
27. Bao, J.; Zhao, L. A review of working fluid and expander selections for organic Rankine cycle. *Renew. Sustain. Energy Rev.* **2013**, *24*, 325–342. [CrossRef]
28. Modi, A.; Haglind, F. A review of recent research on the use of zeotropic mixtures in power generation systems. *Energy Convers. Manag.* **2017**, *138*, 603–626. [CrossRef]
29. Abadi, G.B.; Kim, K.C. Investigation of organic Rankine cycles with zeotropic mixtures as a working fluid: Advantages and issues. *Renew. Sustain. Energy Rev.* **2017**, *73*, 1000–1013. [CrossRef]
30. Zhao, Y.; Liu, G.; Li, L.; Yang, Q.; Tang, B.; Liu, Y. Expansion devices for organic Rankine cycle (ORC) using in low temperature heat recovery: A review. *Energy Convers. Manag.* **2019**, *199*, 111944. [CrossRef]
31. Pethurajan, V.; Sivan, S.; Joy, G.C. Issues, comparisons, turbine selections and applications—An overview in organic Rankine cycle. *Energy Convers. Manag.* **2018**, *166*, 474–488. [CrossRef]

32. Imran, M.; Usman, M.; Park, B.-S.; Lee, D.-H. Volumetric expanders for low grade heat and waste heat recovery applications. *Renew. Sustain. Energy Rev.* **2016**, *57*, 1090–1109. [CrossRef]
33. Calise, F.; Macaluso, A.; Pelella, P.; Vanoli, L. A comparison of heat transfer correlations applied to an Organic Rankine Cycle. *Eng. Sci. Technol. Int. J.* **2018**, *21*, 1164–1180. [CrossRef]
34. Asim, M.; Leung, M.K.; Shan, Z.; Li, Y.; Leung, D.Y.; Ni, M. Thermodynamic and Thermo-economic Analysis of Integrated Organic Rankine Cycle for Waste Heat Recovery from Vapor Compression Refrigeration Cycle. *Energy Procedia* **2017**, *143*, 192–198. [CrossRef]
35. Khalilzadeh, S.; Nezhad, A.H.; Sarhaddi, F. Reducing the power consumption of cascade refrigeration cycle by a new integrated system using solar energy. *Energy Convers. Manag.* **2019**, *200*, 112083. [CrossRef]
36. Nasir, M.T.; Kim, K.C. Working fluids selection and parametric optimization of an Organic Rankine Cycle coupled Vapor Compression Cycle (ORC-VCC) for air conditioning using low grade heat. *Energy Build.* **2016**, *129*, 378–395. [CrossRef]
37. Nasir, M.T.; Ali, M.A.; Khan, T.S.; Al-Hajri, E.; Kadri, M.B.; Kim, K.C. Performance assessment and multi objective optimization of an Organic Rankine Cycle driven cooling air conditioning system. *Energy Build.* **2019**, *191*, 13–30. [CrossRef]
38. Moles, F.; Navarro-Esbrí, J.; Peris, B.; Mota-Babiloni, A.; Kontomaris, K. Thermodynamic analysis of a combined organic Rankine cycle and vapor compression cycle system activated with low temperature heat sources using low GWP fluids. *Appl. Therm. Eng.* **2015**, *87*, 444–453. [CrossRef]
39. Zhai, H.; An, Q.; Shi, L.; Lemort, V.; Quoilin, S. Categorization and analysis of heat sources for organic Rankine cycle systems. *Renew. Sustain. Energy Rev.* **2016**, *64*, 790–805. [CrossRef]
40. LG Centrifugal Chiller. Available online: www.lg.com\T1\guilsinglrightresources\T1\guilsinglrightsac\T1\guilsinglrightLeaflet_F_LG_Centrifugal_Chiller (accessed on 11 August 2021).
41. Toffolo, A.; Lazzaretto, A.; Manente, G.; Paci, M. A multi-criteria approach for the optimal selection of working fluid and design parameters in Organic Rankine Cycle systems. *Appl. Energy* **2014**, *121*, 219–232. [CrossRef]
42. Meng, N.; Li, T.; Wang, J.; Jia, Y.; Liu, Q.; Qin, H. Synergetic cascade-evaporation mechanism of a novel building distributed energy supply system with cogeneration and temperature and humidity independent control characteristics. *Energy Convers. Manag.* **2020**, *209*, 112620. [CrossRef]
43. Yılmaz, A. Transcritical organic Rankine vapor compression refrigeration system for intercity bus air-conditioning using engine exhaust heat. *Energy* **2015**, *82*, 1047–1056. [CrossRef]
44. Rayegan, R.; Tao, Y. A procedure to select working fluids for Solar Organic Rankine Cycles (ORCs). *Renew. Energy* **2011**, *36*, 659–670. [CrossRef]
45. Braimakis, K.; Karellas, S. Energetic optimization of regenerative Organic Rankine Cycle (ORC) configurations. *Energy Convers. Manag.* **2018**, *159*, 353–370. [CrossRef]
46. Bellos, E.; Tzivanidis, C.; Torosian, K. Energetic, exergetic and financial evaluation of a solar driven trigeneration system. *Therm. Sci. Eng. Prog.* **2018**, *7*, 99–106. [CrossRef]
47. Tchanche, B.F.; Papadakis, G.; Lambrinos, G.; Frangoudakis, A. Fluid selection for a low-temperature solar organic Rankine cycle. *Appl. Therm. Eng.* **2009**, *29*, 2468–2476. [CrossRef]
48. Aboelwafa, O.; Fateen, S.-E.K.; Soliman, A.; Ismail, I.M. A review on solar Rankine cycles: Working fluids, applications, and cycle modifications. *Renew. Sustain. Energy Rev.* **2018**, *82*, 868–885. [CrossRef]
49. Xu, J.; Yu, C. Critical temperature criterion for selection of working fluids for subcritical pressure Organic Rankine cycles. *Energy* **2014**, *74*, 719–733. [CrossRef]
50. Brown, J.S.; Brignoli, R.; Quine, T. Parametric investigation of working fluids for organic Rankine cycle applications. *Appl. Therm. Eng.* **2015**, *90*, 64–74. [CrossRef]
51. Chen, G.; An, Q.; Wang, Y.; Zhao, J.; Chang, N.; Alvi, J. Performance prediction and working fluids selection for organic Rankine cycle under reduced temperature. *Appl. Therm. Eng.* **2019**, *153*, 95–103. [CrossRef]
52. Yang, L.; Gong, M.; Guo, H.; Dong, X.; Shen, J.; Wu, J. Effects of critical and boiling temperatures on system performance and fluid selection indicator for low temperature organic Rankine cycles. *Energy* **2016**, *109*, 830–844. [CrossRef]
53. Hærvig, J.; Sørensen, K.; Condra, T. Guidelines for optimal selection of working fluid for an organic Rankine cycle in relation to waste heat recovery. *Energy* **2016**, *96*, 592–602. [CrossRef]
54. Zhai, H.; An, Q.; Shi, L. Analysis of the quantitative correlation between the heat source temperature and the critical temperature of the optimal pure working fluid for subcritical organic Rankine cycles. *Appl. Therm. Eng.* **2016**, *99*, 383–391. [CrossRef]
55. Dai, Y.; Wang, J.; Gao, L. Parametric optimization and comparative study of organic Rankine cycle (ORC) for low grade waste heat recovery. *Energy Convers. Manag.* **2009**, *50*, 576–582. [CrossRef]
56. Chauhan, A.; Vaish, R. Fluid Selection of Organic Rankine Cycle Using Decision Making Approach. *J. Comput. Eng.* **2013**, *2013*, 1–10. [CrossRef]
57. Bolaji, B.O. Performance Study of the Eco-Friendly Hydrofluoroolefins and Dimethyl-Ether Refrigerants in Refrigeration Systems. *Sigurnost* **2014**, *56*, 113–121. Available online: https://hrcak.srce.hr/123976 (accessed on 30 September 2021).
58. Imran, M.; Haglind, F.; Lemort, V.; Meroni, A. Optimization of organic rankine cycle power systems for waste heat recovery on heavy-duty vehicles considering the performance, cost, mass and volume of the system. *Energy* **2019**, *180*, 229–241. [CrossRef]
59. Koç, Y. Parametric Optimisation of an ORC in a Wood Chipboard Production Facility to Recover Waste Heat Produced from the Drying and Steam Production Process. *Energies* **2019**, *12*, 3656. [CrossRef]

60. Rostamzadeh, H.; Ghaebi, H.; Vosoughi, S.; Jannatkhah, J. Thermodynamic and thermoeconomic analysis and optimization of a novel dual-loop power/refrigeration cycle. *Appl. Therm. Eng.* **2018**, *138*, 1–17. [CrossRef]
61. Chagnon-Lessard, N.; Mathieu-Potvin, F.; Gosselin, L. Optimal design of geothermal power plants: A comparison of single-pressure and dual-pressure organic Rankine cycles. *Geothermics* **2020**, *86*. [CrossRef]
62. Gil, B.; Kasperski, J. Performance estimation of ejector cycles using ethers and fluorinated ethers as refrigerants. *Appl. Therm. Eng.* **2018**, *133*, 269–275. [CrossRef]
63. Bekiloğlu, H.E.; Bedir, H.; Anlaş, G. Multi-objective optimization of ORC parameters and selection of working fluid using preliminary radial inflow turbine design. *Energy Convers. Manag.* **2018**, *183*, 833–847. [CrossRef]
64. Moloney, F.; Almatrafi, E.; Goswami, D. Working fluid parametric analysis for recuperative supercritical organic Rankine cycles for medium geothermal reservoir temperatures. *Renew. Energy* **2018**, *147*, 2874–2881. [CrossRef]
65. Imran, M.; Park, B.S.; Kim, H.J.; Lee, D.H.; Usman, M.; Heo, M. Thermo-economic optimization of Regenerative Organic Rankine Cycle for waste heat recovery applications. *Energy Convers. Manag.* **2014**, *87*, 107–118. [CrossRef]